MELİKŞAH ÜNİVERSİTESİ
KAYSERİ

The Graduate Institute of Science and Engineering

M.Sc. Thesis in Material Science and Mechanical Engineering

EFFECT OF BORON ADDITION AND RETAINED AUSTENITE ON THE MECHANICAL PROPERTIES OF HIGH STRENGTH LOW ALLOY (HSLA) SAE 8620 STEEL

by

Munzali MUSA

June 2014
Kayseri, Turkey

EFFECT OF BORON ADDITION AND RETAINED AUSTENITE ON THE MECHANICAL PROPERTIES OF HIGH STRENGTH LOW ALLOY (HSLA) SAE 8620 STEEL

by

Munzali MUSA

A thesis submitted to

the Graduate Institute of Sciences and Engineering

of

Meliksah University

in partial fulfillment of the requirements for the degree of

Master of Science

in

Material Science and Mechanical Engineering

June 2014
Kayseri, Turkey

APPROVAL PAGE

This is to certify that I have read the thesis entitled "Effect of Boron addition and Retained Austenite on the Mechanical Properties of High Strength Low Alloy (HSLA) SAE 8620 Steel" by Munzali Musa and that in my opinion it is fully adequate, in scope and quality, as a thesis for the degree of Master of Science in Material Science and Mechanical Engineering, the Graduate Institute of Science and Engineering, Melikşah University.

_____

June 27, 2014 Prof. Dr. M. Halidun KELEŞTEMUR
Supervisor

I certify that this thesis satisfies all the requirements as a thesis for the degree of Master of Science.

_____

June 27, 2014 Prof. Dr. M. Halidun KELEŞTEMUR
Head of Department

Examining Committee Members

Title and Name		Approved
Prof. Dr. M. Halidun KELEŞTEMUR	June 27, 2014	_____
Yrd. Doç. Dr. Ercan ŞEVKAT	June 27, 2014	_____
Yrd. Doç. Dr. Gökhan ÖZGÜR	June 27, 2014	_____

It is approved that this thesis has been written in compliance with the formatting rules laid down by the Graduate Institute of Science and Engineering.

_____

Prof. Dr. M. Halidun KELEŞTEMUR
Director

June 2014

EFFECT OF BORON ADDITION AND RETAINED AUSTENITE ON THE MECHANICAL PROPERTIES OF HIGH STRENGTH LOW ALLOY (HSLA) SAE 8620 STEEL

Munzali MUSA

M.S. Thesis Material Science and Mechanical Engineering
June 2014

Supervisor: Prof. Dr. M. Halidun KELEŞTEMUR

ABSTRACT

This research work examines the relationship between microstructural characterization and mechanical property of SAE 8620 steel with different contents of boron in ppm rate. SAE 8620 was produced by melting at 1630^{O}C and then supplemented by boron, the casting process give rise to the steel sample with different ppm rate of boron and then rolled. The chemical analyses of the steel were done in TEST KIMYA LAB. 4460 program: G-COZLAB Bursa/Turkey. The studies were conducted in both the as-received state and normalized state with different normalization temperatures within 860^{o}C to 1060^{O}C and different heating time. Hardness of the samples with different normalization temperatures and heating time were measured. Wear test were done to measure the wear resistance, pin-on disk process. The boron inhibits the nucleation of ferrite at the boundary of austenite grain also increasing the depth in which the steel hardened, the hardened specimen have decrease in maximum frictional force and maximum coefficient of friction with increase boron content.

Keywords: SAE 8620 steel, Boron, Normalization, Optical Microscopy, Wear Rate, Friction Coefficient.

YÜKSEK MUKAVEMETLİ DÜŞÜK ALAŞIMLI SAE 8620 ÇELİĞİNİN MEKANİK ÖZELLİKLERİNE BORON İLAVESİ VE KALINTI ÖSTENİTİN ETKİSİ

Munzali MUSA

Yüksek Lisans Tezi – Malzeme Bilimi ve Mekanik Mühendisliği
Haziran 2014

Tez Yöneticisi: Prof. Dr. M. Halidun KELESTEMUR

ÖZET

Bu çalışma SAE 8620 çeliğinin mekanik özellikleri ve mikroyapı ilişkisinin farklı bor oranları (ppm oranında) ile değişimini incelemektedir. SAE 8620 çeliği 1630^{O}C de eritilmiş, oluşan ergiğe farklı oranda (ppm) doğrudan bor katkısı yapılıp dökülmüş ve sonra haddelenmiştir. Kimyasal analiz G-COZLAB 4460 programı ile Bursa Kimya Labaratuvarında yapılmıştır (Türkiye). Çalışmada ısıl işlemsiz malzeme alınıp 860 ^{0}C ile 1060 ^{0}C arasındaki farklı sıcaklıklarda ve bekleme sürelerinde normalizasyon ısıl işlemi yapılmıştır. Farklı normalizasyon sıcaklıkları ve bekleme sürelerinde sertlik ölçülmüştür. Pin-on-disk method ile aşınma direnci ölçülmüştür. Bor ilavesi östenit taneleri sınırında ferrit çekirdeklenmesini ayrıca sertleşme derinliğini artırmıştır, sertleşritilmiş malzeme sürtünme kuvveti boron içeriği artışı ile maksimum sürtünme kuvveti ve minimum sürtünme sabitine sahiptir.

Anahtar Kelimeler: SAE 8620 çeliği, Bor, Normalizasyon, Optik mikroskop, Sürtünme oranı, Sürtünme katsayısı

DEDICATION

This thesis is dedicate to my late father Alhaji Musa Alhassan, who taught me that the best kind of knowledge to have is that which is learned for its own sake. Also, a special gratitude goes to my mother Hajiya Hanne Musa, who taught me that even the larger task can be accomplished if it is done one step at a time.

I also dedicate this thesis to Prof. Munzali Jibril who have supported me througout the process. Special thanks goes to his Excellency the executive governor of Kano State Eng. Dr. Rabiu Musa Kwankwaso (Limamin Kwankwasiyya Amana). My brothers and sisters Hadiza, Alhassan, Nafiu, Ramatu and Shamsuddeen whose encouragement is of paramount importance and push for tenacity in my ears.

I also dedicate this work and give special thanks to Aisha Usman Abdullahi for being there for me throughout the entire masters program. You have been my best cheerleader.

ACKNOWLEDGEMENT

Prof. Dr. M. Halidun KELEŞTEMUR has been the ideal thesis supervisor. His sage advice, insightful criticisms, and patient encouragement aided the writing of this thesis in innumerable ways.

Thanks go to the department members, Prof. Dr. Mahmut D. Mat, Assist. Prof. Dr. Ercan Sevkat, Assist. Prof. Dr. Esad A. Özmetin and Assist. Prof. Dr. Furkar Dundar, for their valuable suggestions and comments. The technical assistance of Hasan Yeşilyurt is gratefully acknowledged.

I express my thanks and appreciation to my family for their understanding, motivation and patience. Lastly, but in no sense the least, I am thankful to all colleagues and friends who made my stay at the university a memorable and valuable experience.

TABLE OF CONTENS

ABSTRACT iii
ÖZ iv
DEDICATION v
ACKNOWLEDGMENT vi
TABLE OF CONTENTS vii
LIST OF TABLES x
LIST OF FIGURES xi
LIST OF SYMBOLS AND ABBREVIATIONS xiv
CHAPTER 1 INTRODUCTION 1
1.1 HIGH STRENGTH LOW-ALLOY (HSLA) STEEL 3
1.2 HEAT TREATMENT OF SAE 8620 4
1.2.1 Conventional Heat Treatment 4
1.2.2 Conventional Heat Treatment of Steel 7
1.2.2.1 Quenching and Tempering Process 7
1.2.2.2 The Effect of Austenitizing Temperature and Time 12
1.2.2.3 The Effect of Tempering Temperature and Time 13
1.3 RETAINED AUSTENITE IN SAE 8620 STEEL 16
1.3.1 The Role of Retained Austenite in Microstructure 17
1.3.2 Retained Austenite Stabilization 18
1.3.3 Behaviour of Retained Austenite 20
1.3.4 Industrial View Point of Retained Austenite 21
1.3.5 Percentage of Retained Austenite Reduction 22
1.3.6 Retained Austenite Analysis 22
1.3.6.1 The Analysis Method 23
1.3.6.2 Areas of Problem 24

1.4 SUB-ZERO HEAT TREATMENT OF SAE 8620 STEEL 24
1.4.1 Cold Treatment for Transformation of Retained Austenite in SAE 8620 Steel..... 24
1.4.1.1 Describing the Heat Treatment Process.....25
1.4.1.2 Increasing Hardness by Transforming Austenite to Martensite in SAE 8620 Steel..... 25
1.4.1.3 Dimensional Stability Improvement 27
1.4.1.4 Cold Treatment before and after Tempering.....27
1.4.1.5 Applications of Cold Treatment.....27
1.4.2 Cryotreatment for Wear Resistance and Dimensional Stability.....28
1.4.2.1 Cryotreatment Introduction 28
1.4.2.2 Processing Cycles for Cryotreatment 30
1.4.2.3 Successful Cryotreatment Applications.....31
1.4.2.4 Unsuccessful Cryotreatment Applications 31
CHAPTER 2: MATERIALS AND METHODS.....32
2.1 MATERIALS.....32
2.1.1 Properties of SAE 8620 Steel 32
2.2 METHODS.....35
2.2.1 Microstructural Examination.....35
2.2.2 Heat Treatment.....35
2.2.2.1 Controlled Cooling.....35
2.2.3 Mechanical Properties 37
2.2.3.1 Hardness 37
2.2.3.2 Wear Test 38
CHAPTER 3: RESULTS AND DISCUSSIONS.....40
3.1 MICROSTRUCTURAL EXAMINATION 40
3.2 HEAT TREATMENT 46
3.2.1 Controlled Cooling.....46
3.2.1.1 Microstructural Examination.....46
3.2.1.2 Hardness 53
3.3 MECHANICAL PROPERTIES.....56

3.3.1 Hardness 56
3.3.2 Wear Test 58
3.3.2.1 Mass Loss for each Test 58
3.3.2.2 Comparison between coefficient of friction of 31, 32 and 33 steel Samples for as-received state with sliding distance of 300m and normal force (F_N) of 5N each 60
3.3.2.3 Comparison between coefficient of friction of 31, 32 and 33 steel Samples with normalization temperature of 960^{O}C, sliding distance of 300m and normal force (F_N) of 10N each 61
3.3.2.4 Comparison between coefficient of friction of 31, 32 and 33 steel samples with normalization temperature of 960°C, sliding distance of 500m and normal force (F_N) of 10N each 62
3.3.2.5 Comparison between coefficient of friction of 31, 32 and 33 steel samples with normalization temperature of 1010°C, sliding distance of 300m and normal force (F_N) of 15N each 63
CHAPTER 4: CONCLUSION 65
REFERENCE…. 67

LIST OF TABLES

TABLE

1.1 Example of Tool Life Improvement Using Cryotreatment 5

1.2 Percentage Increase in Wear Resistance after Cold Treatment and Cryotreatment.6

1.3 Steel Hardness at Various Martensite Percentages for some Low-Alloy Steels ...26

2.1 The Chemical Composition of SAE 8620 Steel 33

2.2 Sample Code with corresponding Boron Content 34

2.3 The Chemical Composition of SAE 8620 Steel 34

2.4 Mechanical Properties of annealed SAE 8620 Alloy Steel without Boron 34

3.1 The three sets of Vickers Microhardness of each Steel Sample and corresponding Cooling Rates.....54

3.2 The average Vickers Microhardness and the corresponding Cooling Rates 55

3.3 Average Brinell Hardness Number (HBN) results of SAE 8620 Steels at various Normalization Temperatures and 45 minutes as Heating Time 56

3.4 Mass Loss (Kg) after each test for the As-received State of Steel Samples.....58

3.5 Mass Loss (Kg) after each test at Normalization Temperature of 960^{o}C for the Steel Samples.....59

3.6 Wear Test Results.....64

LIST OF FIGURES

FIGURE

1.1 Schematic illustration of the formation of pearlite from austenite; direction of carbon diffusion indicated by arrows.....8

1.2 (a) Surface relief and (b) shape change during martensitic transformation.....9

1.3 Simple model for transformation of austenite to martensite.....9

1.4 Dependence of as-quenched hardness on percentage versus martensite and carbon 10

1.5 Continuous-cooling-transformation diagrams for AISI 4340 11

1.6 Microstructure of Steel SS2092 after hardening from (a) 870 (b) 920 (c) 970^{O}C followed by tempering at 200^{O}C.....13

1.7 Effect of Tempering Temperature on the mechanical properties of 1050 steel ...14

1.8 The hardness and impact strength as function of tempering temperature for Cr-Ni-Mo steel.....14

1.9 Tensile and yield strength and ductility versus tempering temperature for AISI 4340 steel 15

1.10 Effect of time at four tempering temperatures on a hardness of 0.82% carbon steel……..……..16

1.11 Balancing properties and Retained Austenite content…….……21

1.12 Diffraction pattern used for retained austenite analysis.....23

1.13 Effect of Carbon Content on M_s and M_f temperatures.....26

1.14 Heat Treatment Sequence for Maximum Transformation of Austenite to Martensite. 27

1.15 Effect of cooling to sub-zero Temperature on Carbide Number for D2 Steel. Austenitizing Temperature of 970, 1010, 1040 and 1070^{o}C were used before hardening process 29

1.16 Effect of Holding Time at -196^{o}C (-320^{o}F) on Carbide Number for D2 Steel. Carbides were measured using optical Techniques 29
1.17 Effect of Austenitizing Temperature and Holding Time at Cryogenic Temperature on Hardness of D2 Cold-Work Tool Steel.....30
1.18 Influence of Temperature on Wear Rate for D2 Steel.....30
2.1 High Temperature Microscope Stage (with ceramic heating element made of Pt/Rh thermocouple 7/3 cup) 36
2.2 Controlled Cooling Process Experimental Set-up.....37
2.3 Nanovea Tribometer Test Machine Experimental Set-up.....39
2.4 Mass Test Machine.....39
3.1 Optical micrographs of as-received state of (a) 3.3 ppm (b) 13.5 ppm (c) 29.6 ppm (d) 43.7 ppm (e) 58 ppm boron steel samples.....41
3.2 Optical micrographs of SAE 8620 steel with 3.3 ppm of boron and normalization at 960^{O}C for (a) 45 minutes and (b) 60 minutes heating time 42
3.3 Optical micrographs of SAE 8620 steel with 3.3 ppm of boron 45 minutes heating time and normalization temperature of 1010^{O}C.....42
3.4 Optical micrographs of SAE 8620 steel with 13.5 ppm of boron 45 minutes heating time and normalization temperature of 1010^{O}C.....43
3.5 Optical micrographs of SAE 8620 steel with 29.6 ppm of boron, normalization temperature of 960^{O}C and waiting time of 60 minutes (a) 200× magnification (b) 400× magnification.....43
3.6 Optical micrographs of SAE 8620 steel with 29.6 ppm of boron 45 minutes heating time and normalization temperature of 1010^{O}C.....44
3.7 Optical micrographs of SAE 8620 steel with 43.7 ppm of boron and normalization temperature of 960^{O}C (a) 45 minutes heating time (b) 60 minutes heating time..45
3.8 Variation of austenic grain sizes with respect to austenitization temperatures for 15BCr30 and PL22 steels: (a) and (d) 870^{O}C, (b) and (e) 1050^{O}C, (c) and (f) 1200^{O}C 45
3.9 Microstructure images of 3.3 ppm of boron (31 steel) steel sample with 20^{O}C/min cooling rate 46

3.10 Microstructure images of 3.3 ppm of boron (31 steel) steel sample with 70^{O}C/min cooling rate 47
3.11 Microstructure images of 3.3 ppm of boron (31 steel) steel sample with 130^{O}C/min cooling rate 49
3.12 Microstructure images of 13.5 ppm of boron (32 steel) steel sample with 20^{O}C/min 50
3.13 Microstructure images of 13.5 ppm of boron (32 steel) steel sample with 70^{O}C/min.....50
3.14 Microstructure images of 13.5 ppm of boron (32 steel) steel sample with 130^{O}C/min.....51
3.15 Microstructure images of 29.6 ppm of boron (33 steel) steel sample with 20^{O}C/min cooling rate 52
3.16 Microstructure images of 29.6 ppm of boron (33 steel) steel sample with 70^{O}C/min cooling rate 52
3.17 Microstructure images of 29.6 ppm of boron (33 steel) steel sample with 130^{O}C/min cooling rate.....53
3.18 Graph of Vickers microhardness (HV) against cooling rate (^{O}C/min) for 3.3 ppm, 13.5 ppm and 29.6 ppm of boron.....55
3.19 Graph of Brinell hardness (HBN) of SAE 8620 steels against normalization temperatures of 860^{O}C, 900^{O}C, 960^{O}C, 1010^{O}C and 1060^{O}C.....57
3.20 Graph of Brinell hardness against Boron content.....58
3.21 Graphs of mass loss (Kg) against sliding distance for each test for the as-received State and normal force of 5N.....59
3.22 Graph of mass loss against corresponding sliding distance at normalization temperature of 960^{O}C.....60
3.23 The graph of coefficient of friction against sliding distance of 31, 32 and 33 steel samples for as-received state, with a sliding distance of 300m and normal force (F_N) of 5N 61
3.24 The graph of coefficient of friction against sliding distance of 31, 32 and 33 steel samples with normalization temperature of 960^{O}C, sliding distance of 300m and normal force (F_N) of 10N.....62

3.25 The graph of coefficient of friction against sliding distance of 31, 32 and 33 steel samples with normalization temperature of 960°C, sliding distance of 500m and normal force (F_N) of 10N 63
3.26 The graph of coefficient of friction against sliding distance of 31, 32 and 33 steel samples with normalization temperature of 1010°C, sliding distance of 300m and normal force (F_N) of 15N 64

LISTS OF SYMBOLS AND ABBREVIATIONS

SYMBOL/ABBREVIATION

V_8	Volume of Austenite
V_m	Volume of Martensite
W_R	Abrasive Wear Rate
K	Wear Coefficient
V	Sliding Velocity
F	Normal Force
HSLA	High Strength Low-Alloy
M_s	Martensite Start Temperature
M_f	Martensite Finish Temperature
FCC	Face Centered Cubic
BCC	Body Centered Cubic
BCT	Body Centered Tetragonal
CCT	Continuos Cooling Transformation
AISI	American Iron and Steel Institute
RA	Retained Austenite
T_q	Quenchant Temperature
HBN	Brinell Hardness Number
HV	Vickers Hardness
MPa	Mega Pascal

CHAPTER 1

INTRODUCTION

In this research work, famous HSLA (High Strength Low-Alloy) Steel well known as SAE 8620 with different boron content was investigated, which is introduced briefly as follows. SAE 8620 is a hardenable Nickel (Ni), Chromium (Cr), and Molybdenum (Mo) low-alloy steel often used in bearings, automotive gearing, automotive body components and transmission components of cars applications. Its mechanical properties includes Tensile strength of 650-880 MPa, Young's modulus of 200-200 GPa, Fatigue life of 275-275 MPa, Yield strength of 350-350 MPa and elongation of 8-25%. Also, some of its physical properties include thermal conductivity of 25-25 W/m.k, melting temperature of 1450-1510 ^{O}C, with density of 7700-7700 Kg/m^3 and resistivity of 0.55-0.55 ohm.mm^2/m.

These boron steels nowadays have wider range of applications and more diversity in their applications. With their effective and high mechanical properties, at an affordable cost, are achieved by advanced manufacturing technology as a result of enough knowledge of manufacturing materials. Despite the fact that these boron steels were contrive mainly for hard and wear-resistant elements, presently they are also called to public attention for other wider applications. For example, the boron steel grade B27, manufactured by a well known company, as one of the typical steel of the boron steel group [1]. The high efficiency of this microalloying element boron is explained with the following reasons of its small atomic radius and also very low solubility in iron, which makes it to concentrate (condense) primarily on the austenite grains boundaries, which attract various structure faults, lowering the energy of the boundaries and the chance of possibility of creating crystallization centers, which directly increase the steel hardenability [2]. The highest presences of boron at boundaries of austenite grains have been proven experimentally [3].

This experimental work shows that only the boron that goes in as solid solution exerts a positive effect on the hardenability [4]. The percentage concentration of soluble boron that goes in as a solid solution should be 8ppm (0.0008%) minimum for effective increase in the hardenability [5]. Considering the presence of this element boron and diminishing the energy of grain boundaries, then assumptions will be made that the largest amount of boron will be seen in areas with multiple faults, where the constitution of ferrite is the most likely. Hence, maximum hardenability in boron steel with explicitly composition in particular hardening conditions is achieved if the cognitive content of soluble boron did not surpass that needed for the decrease of the boundaries energy in areas having ferrite constitutions [6]. Addition of slight amount of boron microalloying element to steels slows down the austenite to ferrite transformation and consequently the hardenability tends to improve in HSLA steels and thereby production cost becomes cheaper [7-10]. It is well known from literature that uttermost hardenability of these HSLA steels is attained within the range of 20-30 ppm of boron [11].

Unspecified number of industries regarded retained austenite as highly unsuitable in component parts of tooling equipment and die industry. Premature failures in automobile body components, structural and other applications of HSLA steels is caused by excess presence of retained austenite. Low hardness of retained austenite is also another factor that mismatched with most applications that require high wear resistance properties by inhibiting the hardness to maximum attainable state. Tempering is a vital process in transformation of these retained austenites to martensite. An important point is holding at sufficient time and temperature. To ensure maximal or greatest amount of retained austenite is transformed to martensite, more than one temper is often done. Other techniques regarded with favor are cold treatment at -120^{O}F (-85^{O}C) and cryogenic treatment at -320^{O}F (-195^{O}C). Many literature shows that high percentage of transformation to martensite is achieved by lowering the cold treatment temperature [12], i.e., the percentage of retained austenite is reduced. By regulating the amount of this retained austenite, its good and enhancing well-being properties can be actualized without having any miserable effect from its negative perspective, like excessive dimensional growth. A good number of industries enjoy the profit driven from retained austenite content to attain equilibrium of fatigue life, impact strength and dimensional stability [12]. The most desirable amount of

retained austenite involves balance of regulations and must consider properties like its material composition and heat treatment process diversity. These diversities in the material composition and heat treatment includes steel chemistry, carbon rate (in weight %), austenitization and tempering temperatures (^{O}C) and quenching rate (^{O}C/min) [12].

1.1 HIGH STRENGTH LOW-ALLOY (HSLA) STEELS

HSLA (High Strength Low-Alloy) steels are typically micro alloyed steels that render excellent mechanical properties and high degree of corrosion resistance properties when compared to carbon steels. HSLA steels differ from other classes of steels, i.e. they are made to compromise with particular mechanical properties rather than to compromise particular in steel chemical composition. Their carbon contents in weight percentage varied between the range of 0.05-0.25% to maintain weldability and formability. Other alloying elements in HSLA steels constitute of 2.0% manganese and little quantities (in weight percent) of copper, nickel, niobium, nitrogen, vanadium, chromium, molybdenum, titanium, calcium, rare earth elements or zirconium [13][14]. The alloying elements such as copper, titanium and vanadium are added intentionally for strengthening purposes [14]. The alloying elements are planned to modify (change) the microstructural characterization of carbon steels, often known to be a ferritic-pearlitic aggregates, to give rise to a very fine dispersion of alloy carbides in nearly perfect ferrite matrix. For ferrite, the increase in yield strength is between the ranges of 250 to 590 megapascals. HSLA steels possess higher mechanical properties of strength and toughness and normally need 25-30% greater extent power to form, when compared to corresponding carbon steels [14].

The corrosion resistance properties of HSLA steels are increased by the addition of these alloying elements: nickel, chromium, copper, silicon and phosphorus. Most HSLA steels have the properties of directionally (guiding) sensitive properties and need these alloying elements. Other properties like formability and impact strength may vary in a significant manner when the grains are proved transversely and longitudinally. In parallel to the longitudinal grain, the bends have more tendencies to crack in the vicinity of outer edge due to tensile loads. This directional characteristic is considerably reduced in HSLA steels that have been treated for sulfide shape control [14].

They are of paramount importance in applications that are required to deal with large amounts of stress and good strength-to-weight ratio such as cranes, cars, bridges, roller coasters trucks and other structural applications [15][16].

The resistances to rust properties in high strength low-alloy steels are more when compared to carbon steels due to the facts that carbon steel does not have the pearlite phase. HSLA steels usually have densities of around 7800kg/m^3 [17].

1.2 HEAT TREATMENT OF SAE 8620

1.2.1 Conventional Heat Treatment

Heat treatment of metals has changed from old age technologies (black art) to advanced technologies of modern science over centuries. Phase diagrams and heat treatment process cycles have been developed as a result of intensive international research work. Metallurgist understands the scope of how, why and when metal alloys reacts to heat-treatment process. Also they understand changing any of the process variables like austenitizing temperature, cooling and quenching rate and tempering temperature will greatly alter the final properties of the metal alloy.

The low temperature heat treatment process is under studies recently with great research on sub-zero cooling process. For the past decades, sub-zero treatment of metals is in the state of high esteem and honor to rapid fix for misfortunate heat treatment process. Metal industries have no adoptive sub-zero processing technology because of inadequate knowledge of the cardinal and underlying metallurgical mechanisms and also wide variation in literatures and research findings. Recent claims that cryogenic treatments can work out every state of difficulty that needs to be resolved have paramount lessened the interest of research in cryogenics as a believable process. The key to understanding of the mechanisms governing sub-zero process have been studied by Dr. Randall Barron at the University of Louisiana was one of the pioneers in conducting significant research [18] [19]. into sub-zero processing. His research shows that sub-zero processing of steels can improve various properties including:

- Hardness and strength
- Wear resistance
- Dimensional stability

"As an earlier proponent of sub-zero processing corrugated board industry has achieved significant improvements in wear resistance for different types of cutting tools. Trimmers, cutting knives, score cutters, bracket trimmers, chipper knives and envelope dies have increased their useful life by factors of 2 to 5" [20-25].

Table 1.1 shows the improvement in the average life of special pieces with and without the process of sub-zero treatment. This improvement is explained with the term wear ratio, and is defined as the ratio of life after sub-zero treatment by the average tool life without sub-zero treatment; this gives explanations on the amount of improvement after cryotreatment when done in the proper mode.

Table 1.1: Example of Tool Life Improvement Using Cryotreatment [19, 20, 22, 27].

Tooling	Life before treatment (Average)	Life after Cryotreatment (Average)	Wear ratio
5-cm end mills used to cut C1065 steel	65 parts	200parts	3.07
Hacksaw blades used to cut bosses on M107 shells	4h	6h	1.5
Blanking of heat treated 4140 and 1095 steel	1,000 pieces	2,000 pieces	2.0
Broach used on a C1020 steel torque tube	1,810 parts	8,602 parts	4.75
Gang milling T-nuts from C1018 steel with M2 Cutters	3 bars	14 bars	4.67
AMT-38 cut-off blades	60h	928h	15.4
Nosing thread dies used in metal working	225 shells	487 shells	2.12

$$\text{Wear ratio} = \frac{Life\ After\ Treatment}{Life\ Before\ Treatment} \quad \text{.....Eq. 1}$$

Table 1.2 shows variations in wear life when compared between parts that are cold treated at cold treatment temperature of about -80^0C (-110^oF), and parts cryogenically treated at -190^0C (-310^oC) with liquid nitrogen as the coolant, considerable improvement in

Table 1.2: Percentage Increase in Wear Resistance after Cold Treatment and Cryotreatment [26].

US steel designation and At -190^{O}C (-310^{O}F)			Description	At -79^{O}C (-110^{O}C)
AISI(USA)	DIN(BRD)	Materials with high improvement	In percent	In percent
D2	1.2379	High carbon/chromium steel	316	817
S7		Silicon tool steel	241	503
52100	1.3505	Bearing steel	195	420
01	1.2510	Oil hardening cold work die steel	221	418
A10		Graphite tool steel	230	264
M1	1.3346	Molybdenum high speed steel	145	225
T1	1.3355	Tungsten/molybdenum HSS	117	203
CPM 10V		Alloy steel	94	131
P20	1.2330	Mold steel	123	130
440		Martensitic stainless steel	128	121
Materials without significant improvement				
430		Ferritic stainless steel	116	119
303	1.4305	Austenitic stainless steel	105	110
8620	1.6523	Case hardening steel	112	104
C1020	1.0402	0.20% carbon steel	97	98
AQS		Grey cast iron	96	97

the wear resistant properties are achieved. Nevertheless, from these studies the net result obtained could not be subject to disagreement and debate but more researches have been conducted to gain a better understanding of the fundamental mechanisms.

1.2.2 Conventional Heat Treatment of Steel

One of the mechanisms to strengthen and harden most steels such as low-alloy, carbon and tool steels is heat treatment in which controlled amounts of martensite are produced in the microstructure. Heat treatment in steel tends to change the mechanical properties like steel impact and tensile strength, hardness, fatigue life and its toughness. With this, careful control of the microstructure of a specific steel alloy system is practically explained by the Iron-carbide (Fe_3C) phase diagram. Most microstructures are developed as a result of phase changes (transformations): the changes that happen between phases upon subsequent heating or cooling, but mostly cooling. Heat treatment of steel begins with heating up the steel to austenitizing temperature, according to the Fe_3C phase diagram (soft and tough phase) is produced and also this austenite is a stable phase. Next process involves cooling down to a suitable temperature depending upon the alloy content. The type of a heat treatment process to be done mostly depends on the desired microstructures and the steel composition (steel alloying element composition). Also, subsequent cooling rate plays a great role in the resultant structure and properties [28].

1.2.2.1 *Quenching and Tempering Process*

Quenching or rapid cooling results in the hardening of the steel. After cooling the austenite is unstable and will further transform to different phases like martensite, pearlite, and bainite according to the cooling condition, i.e. either slow cooling or fast cooling conditions. In slow cooling rates, diffusion usually controls the transformation; in plain carbon steels, phases like pearlite or bainite are formed, through a so called “diffusional transformation”. In this kind of transformation, diffusion (especially that of carbon) plays the main role in the nucleation process and grain-growth stage, which in turn is carefully controlled by temperature and time. By slow cooling of austenite to the temperature range of 600-700^{O}C, ferrite and cementite phases are formed and start to nucleate on the existing austenite grain boundaries. If in the same temperature range, time is given to the steel, these nuclei grow to form a special microstructure called pearlite, as indicated schematically in Figure 1.1

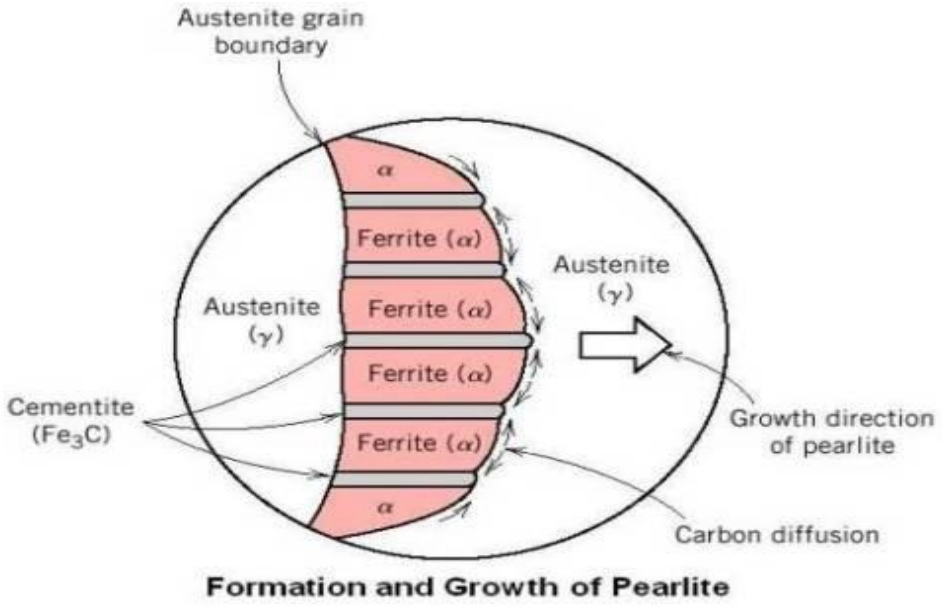

Figure 1.1: Schematic illustration of the formation of pearlite from austenite; direction of carbon diffusion indicated by arrows [37].

Consequently, if the austenite is cooled rapidly from the austenitizing temperature, martensite phase will be formed predominantly through a process called "a thermal or diffusionless transformation" [29]. Ms (martensite start temperature) and M_f (martensite finish temperature) are the two main temperatures in the martensite transformation. But below Ms, the free energy of the metal is lowered if the metal changes its phase from that stable at high temperatures to that stable at low temperature. This free-energy difference is a primary driving force for a martensitic reaction [30].

If the final temperature falls down to a temperature between Ms and M_f, the structure formed is the martensite phase. The martensite phase transformation occurs by a cooperative atomic arrangement. In this way, atoms in the parent austenite lattice are re-aligned into the lattice of the martensite phase [29]. In carbon steels the martensitic transformation involves a structure change from a FCC (Face Centered Cubic) crystal lattice (FCC austenite) to a BCT (Body Centered Tetragonal) martensite or highly distorted BCC crystal structure. The atomic re-arrangement associated with the martensite reaction produces a shape deformation, as shown schematically in Figure 1.2. The habit plane, or plane on which martensite plates form, is assumed to be the undistorted plane. The strain of

this deformation is known as the invariant-plane strain [30]. In the mechanism of the martensite formation, there are considerable controversies and several theories.

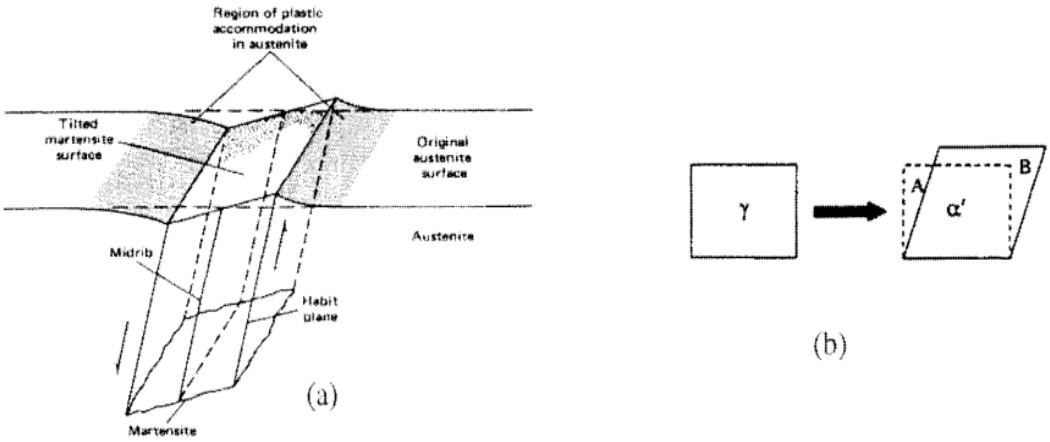

Figure 1.2: (a) Surface relief [31] and (b) shape change during martensitic transformation.

A simple model of martensite transformation suggested by Bain [32] is shown in Figure 1.3. The carbon atoms situated on the edges of the martensite unit cells cause the unit cell to increase in one direction, which results in a tetragonal lattice.

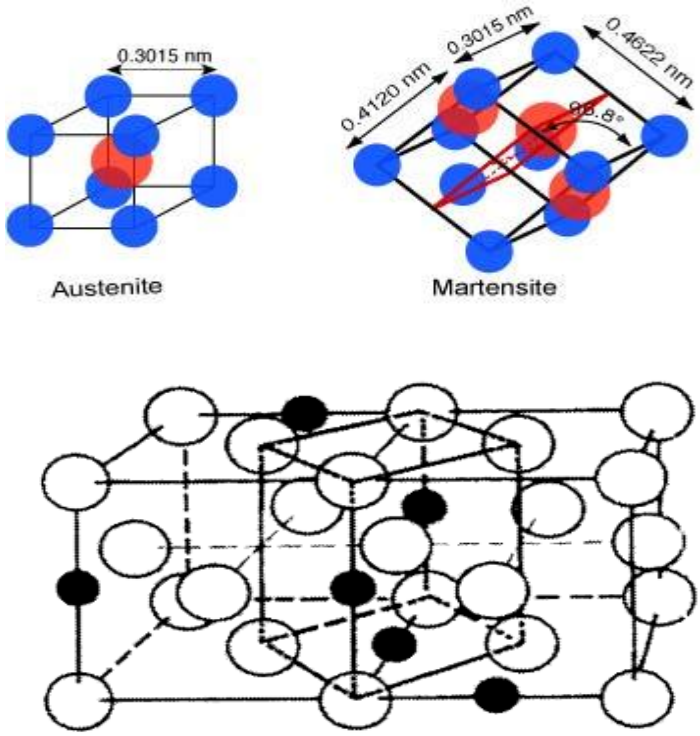

Figure 1.3: Simple model for transformation of austenite to martensite [32].

As mentioned earlier, by fast cooling down to a temperature below Ms, there is every opportunity for carbon to diffuse out of the austenite lattice. Thus, the carbon atoms remain in the Fe solid solution. Since the space available for the carbon atoms is not sufficient, they expand the lattice to BCT. One of the major characteristics of martensite is the existence of many defects in the lattice. In low carbon steels, for instance, hardness results from the high dislocation density, whereas at higher carbon level, carbon interstitial solid solution strengthening is dominant [33, 34]. Figure 1.4 shows the dependence of hardness on martensite volume fraction and carbon content of steel.

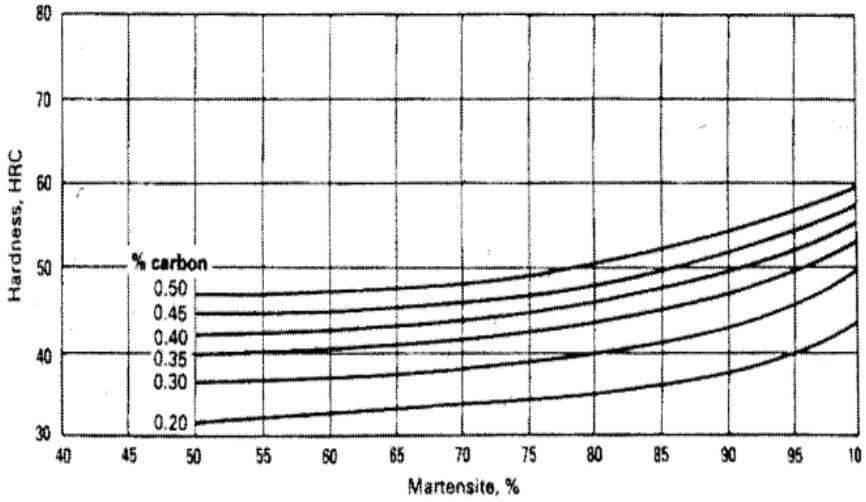

Figure 1.4: Dependence of as-quenched hardness on percentage versus martensite and carbon [31].

At each point in time, it should be noted that when the hardness of steel is improved by the process of martensite formation, it will be accomplished by scarifying toughness. And the entire process is as a result of high increase in the total internal-energy due to the defects.

Harder martensitic phase can be achieved by increasing the alloy content and carbon content of the austenite, and hence increasing either austenitizing temperature or the holding time, and consequently lowering the Ms and M_f temperatures. Therefore, the transformation from such reinforced matrix to martensite phase is accomplished to a greater extent deformation strain stash away in the martensite lattice, leading to a greater extent

lattice defects, harder and stronger martensite. This martensite phase is harder due to the fact that more solid solution effects of carbon and alloying elements [35].

The second phase for the hardenability of steel is the quenching process. The most widely used quenching techniques are in the form of liquid or gas and sometimes molten salt can be used. The liquid quenchants are water, oil, polymer solutions in aqueous form and water mixed with some amount of salt. The gaseous quenchants are air (normalization process), and inert gases including nitrogen, argon and helium. As cited earlier, cooling rate from the austenite region to room temperature defines the type of end microstructure and this can be shown from CCT (Continuos Cooling Transformation) phase diagrams [36]. The CCT diagram for AISI 4340 steel is shown in figure 1.5. From the figure, it shows clearly that fully martensitic microstructure phase in this alloy steel requires cooling rate that is faster than 8.3^{O}C/s from the austenitizing temperature [37].

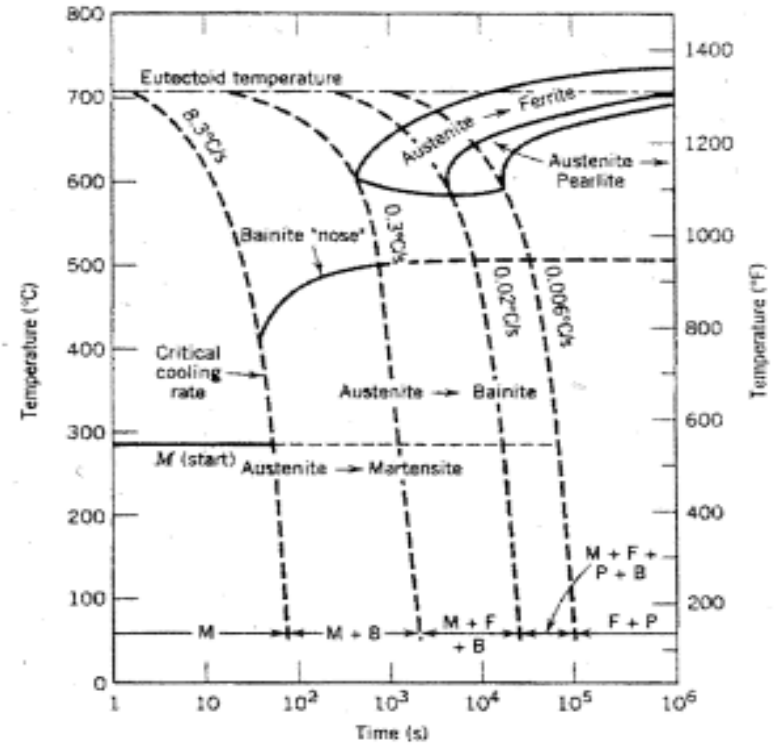

Figure 1.5: Continuous-cooling-transformation diagrams for AISI 4340 [37].

Brittleness of steel problem is solved by ***tempering*** and is the next process after the quenching process. In this procedure, the steel sample is heated to a certain temperature less

than the austenitizing temperature between 160^{O}C and 650^{O}C for some heating time of 30 min to 4 hours. “Tempering of steel can be defined literary as the process whereby hardened or normalized steel is heated to a temperature below the critical temperature, and then cooled at a suitable rate, mostly to increase ductility and toughness, moreover and to ensure dimensional stability”. Other important usage of the tempering process includes relieve stresses from forming and machining, and also bring down the hardness resulting from welding.

In steels consisting of predominantly martensitic microstructure phase, the Fe lattice in it is strained by interstitial carbon atoms and its hardness is significantly increased. By heating during tempering process, the interstitial carbon atoms diffuse and form but through some steps, an alloy carbide or Fe_3C in a ferrite matrix, leading to a gradual decrease in the above-mentioned lattice strain. After tempering, the final products have some properties which depend on shape, size, alloy composition and the carbides distribution that forms. The consequent changes in the morphology in microstructure decrease hardness, yield and tensile strengths but increase ductility and toughness. Tempering process of steels that are hardened with precisely very low degrees of temperatures is likely to cause no important changes in hardness, rather may ultimately increase the yield strength [38, 39].

1.2.2.2. *The Effect of Austenitizing Temperature and Time*

Each steel grade according to literature and practical experiences posses a range of temperatures for austenitizing before the hardening process. The temperature range of some or all the carbon and the alloying elements are dissolved. Grain growth happens with drastic increase in austenitizing temperature and also the retained austenite content after the rapid cooling process (quenching) increases. This verified information can be shown in Figure 1.6. At 920^{O}C and 970^{O}C the retained austenite may be distinguished as light angular areas [32].

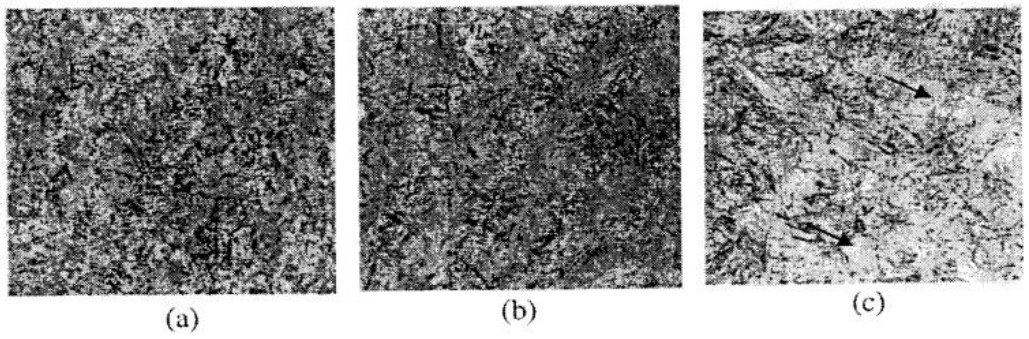

Figure 1.6: Microstructure of steel SS2092 after hardening from (a) 870 (b) 920 (c) 970^{O}C followed by tempering at 200^{O}C [32].

With the steel attaining its austenitizing temperature, the microstructural phase is called the austenite phase and is a soft but tough phase. The time of holding at this austenitizing temperature depends greatly on the amount carbides dissolution and grain size. For the fact that the amount of carbide differs for each type of steel, also holding time will also varied accordingly to the steel grade. Example, for a few minutes holding time is adequate for low-alloy structural steels and plain-carbon steels as they comprise of easily dissolved carbides. In the present steels, to ensure sufficient carbide dissolution, a holding time of 5 to 15 minutes is sufficient, whereby as for medium-alloy structural steels a corresponding holding time of 15 to 25 minutes is sufficient too [32].

1.2.2.3 *The Effect of Tempering Temperature and Time*

Temperature and time are very important parameters in tempering process and are so closely related variables. But varying the temperature has the greatest effect compared to variations in holding time in a typical tempering operation. Figure 1.7 shows the effect of tempering temperature on hardness, tensile and yield strengths, elongation and reduction in area of plain-carbon steel which has 0.52% carbon. From the figure both hardness and strength properties tends to decrease in magnitude as the tempering temperature is increased. Most medium-alloy steels are affected by the tempering process almost in the same manner as this carbon steel [38, 39]. When incorrect tempering temperatures is done in carbon steels, loss in toughness happens compared to the normal tempering cycle and it should be avoided. This phenomenon, temper embrittlement, can be shown in Figure 1.8

for a type Cr-Ni-Mo steel (SS2550) by the drop in impact strength, which is very similar to toughness [32].

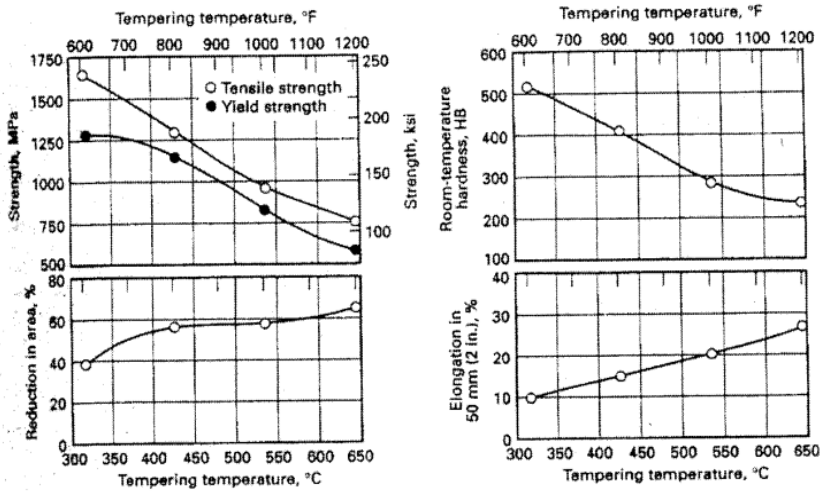

Figure 1.7: Effect of tempering temperature on the mechanical properties of 1050 steel [38].

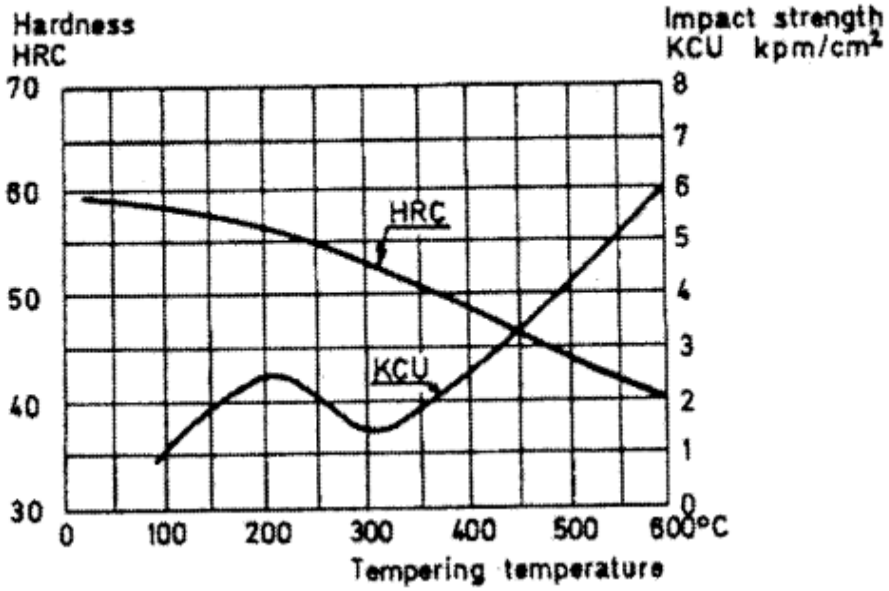

Figure 1.8: The hardness and impact strength as function of tempering temperature for Cr-Ni-Mo steel [32].

For AISI (American Iron and Steel Institute) 4340, a variation in mechanical properties against tempering temperature as shown in Figure 1.9. As explain earlier, by

increasing the tempering temperature, tensile and yield strengths decrease against the increase in reduction area as a measure of ductility [37].

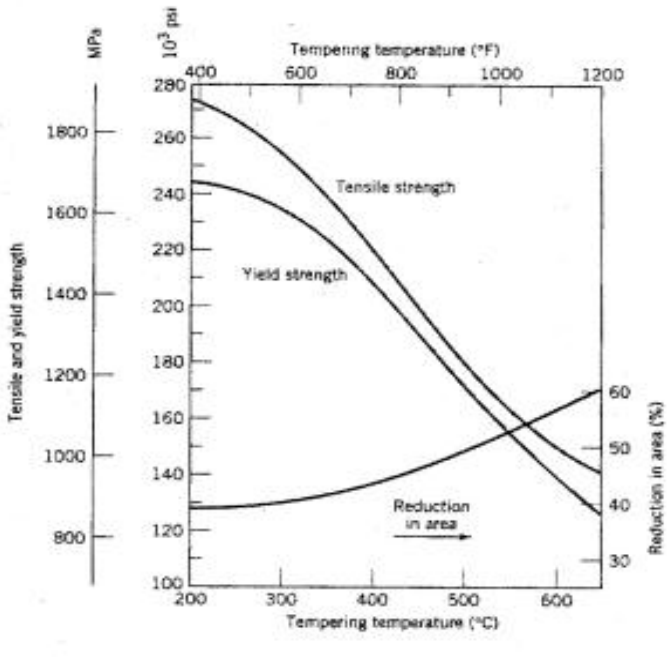

Figure 1.9: Tensile and yield strength and ductility versus tempering temperature for AISI 4340 steel [37].

Time is also another vital parameter in tempering process of steel. Carbides are formed by diffusion process of carbon and alloying elements depends on both tempering temperature and time. The result of tempering time on the hardness of carbon steel at various temperatures is shown in Figure 1.10. It can be seen that the variations in hardness are approximately linear over a large part of the time range if the time is presented on a logarithmic scale [38].

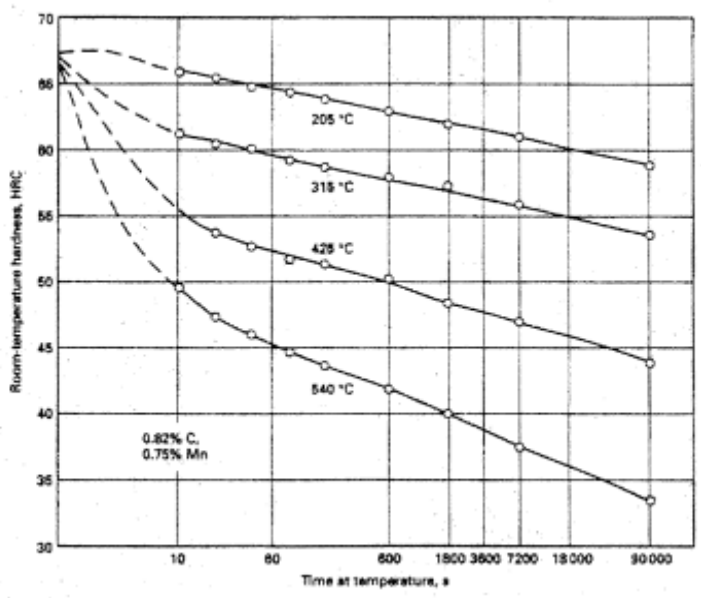

Figure 1.10: Effect of time at four tempering temperatures on a hardness of 0.82% carbon steel [38].

1.3 RETAINED AUSTENITE IN SAE 8620 STEEL

RA (Retained austenites) are austenite that does not transform to martensite upon quenching (rapid cooling). Thus, RA occurs when steel is not quenched to the M_f, that is, low enough to form 100% martensite. Because the M_f is below room temperature in alloys containing more than 0.30% carbon. These RA are specialized crystalline form of iron and steel. Thus, the percentage in quantity of RA in a steel microstructure depends on some contents and processes such as carbon content in the steel, alloying element content (particularly manganese and nickel), final quenching temperature and corresponding mechanical treatments [40].

At a specific temperature (M_s), austenite begins its transformation to martensite upon rapid cooling (quenching). This transformation upon quenching depends on the steel chemical composition. The M_s can be obtained from many equations, among is the Steven and Haynes formula [41], Equation 2.

$$M_s\,(^{O}C) = 561\text{-}474C\text{-}33Mn\text{-}17Ni\text{-}17Cr\text{-}21Mo \quad \text{.....Eq. 2}$$

The above mentioned equation is reasonable for steel with a maximum content of 0.6 %C and the alloying elements quantities are given in weight percentages [41]. Two sets of temperatures, which are M_s and the Tq (quenchant temperature), explain greatly about the volume of untransformed austenite to martensite. Koistinen and Marburger define this relation by:

$$V_8 = e^{-1.10\times\exp(-2)(M_s - T_q)} \quad \text{.....Eq. 3}$$

The amount of martensite is $V_m=1-V_8$. According to equation 3, the amount of formed martensite is not a function of time [42].

In microstructure of steels, the RA appears as occasional patches in the microstructure of conventional heat treated steel and as well as that of cold treated steel samples [43]. Well known techniques such as the X-ray diffraction, quantitative optical metallography, electric resistance, dilatometer and thermal analysis are used to measure the amount of this retained austenite in steels microstructure. Also, austenite that is stable during the transformation process can be measured by these techniques, but with the exemption of X-ray diffraction and metallography methods. The metallography methods are usually not practical due to constrains such as difficulties of observing different phases and also require more researching time [44].

In his study, Osman ASİ, states that "test results obtained shows that highest percent content of RA is in the microstructures of the carburized specimens that are carburized 45 minutes, 3 hours and 5 hours carburizing times of 940^{O}C each were 35.8%, 19.4% and 15% respectively" [45].

1.3.1 The Role of Retained Austenite in Microstructure

RA plays an important role because it has both positive and negative effects on the properties and performance of steels, and so these properties make it so complex. High content of RA leads to these properties: lower elastic limits, reduced hardness and dimensional stability. However, low content of it results to: poor fracture toughness and reduced low cycle fatigue life [46].

When steel are heat-treated, they could contain a reasonable amount of volume fraction of RA and relies greatly on the steel chemical composition, austenitization temperature, final quenching temperature, quenching rate and the stress rate. The ability to control the properties of steel and ensuring their good quality by determining the amount of this RA in heat-treated steels by X-ray diffraction plays an important role. The properties that give RA most of its singular properties are those responsible for significant problems in most applications, it is well known that the normal phase (state) of steel at high temperature is the austenite phase. RA is also metastable (can change from austenite to ferrite depending on the condition) when it exist outside of its normal range of temperature. Furthermore, increase in volume goes along with this transformation and creates internal stress in a component, and leading to cracks [46].

1.3.2 Retained Austenite stabilization

Paul Stratton and Cord Henrik Surberg state that "case-hardening components made of low-alloy steels often have RA in the case after quenching, which can be transformed to martensite by further cooling of the component, even if the austenite stabilizes during aging at room temperature".

The stabilization process of retained austenite in steel tooling applications is well documented [47, 12]. Austenite is retained in the microstructure of quenched steel with M_f that is below room temperature. If the cooling process is instantly continued to a temperature below the M_f, almost all the austenite present at room temperature can be transformed to martensite. Nevertheless, delay in quenching between room temperature and further cooling can result to stabilization of the austenite and cannot be further transformed by subsequent cooling [48]. Literature shows that RA causes cracking during grinding after heat treatment processes.

Variations of reports in literature states that stabilization process does not happen in carburized low alloyed steels [49]. However, some reports states that stabilization does occur [50, 51], and some reports states that its onset is very rapid [52]. Reports from literature that proves the occurrence of stabilization shows that it is generally connected

with high alloy content, mostly alloying element nickel, and with nitrogen in some instances.

Stabilization of RA is achieved by a mechanism called the pinning mechanism. Carbon atom is redistributed by diffusion out of the martensite during aging process. The stabilization of the structure is achieved by interstitial carbon atoms pinning the austenite-martensite interface [50]. As the pinning mechanism increase with more time after quenching, a greater extent of energy is needed to resume the transformation from austenite to martensite, this means that a lower cold treatment temperature is needed for the mechanism [53].

It is well proved that some alloying elements addition in steel mostly nickel, carbon, and nitrogen boost (advanced) stabilization [50, 54].

Literature shows that carburized steel of SAE 8620, cold treated temperature of -120^{O}C is enough to restart RA to martensite transformation after any stabilization period of time. The temperature range of -40 to -70^{O}C is enough to restarts this RA to martensite transformation after stabilization process.

The result of the study compiled with other results from previous studies develops a certain number of recommendations for cold treatment process of case carburized components. These recommendations state that, the following steps should be adopted to eliminate RA:

- The higher the alloy content (particularly nickel), the shorter the stabilization time and the lower the cold treatment temperature that should be used.
- The higher the case carbon content, the shorter the stabilization time and the lower the cold treatment temperature that should be used.
- The shorter the delay between quenching and cold treatment the better.
- The colder the treatment temperature the better.

1.3.3 Behavior of Retained Austenite

Martensite phase is characterized to be a hard, strong and brittle phase while austenite phase is characterized to be soft and tough. In some cases, when austenite and martensite are combined forms a composite material that posses some benefits of each, and also compensating for the defects of both. High percentage of RA content affects the mechanical properties of most applications, because this austenite is soft as mentioned earlier. For example, properties like dimensional stability, fatigue life and impact strength of bearing steels are affected by RA content [40].

- Dimensional stability: Transformations from RA to martensite will occur if temperature drops rapidly below the lowest temperature to which it was quenched or by mechanical stress. The BCT crystal structure (martensite), possessed larger volume than the FCC crystal structure (austenite) that replaces it. A localized increase in 4-5% in the volume of the microstructure at room temperature where transformation occurs, and a resulting dimensional change could pave way to growth and most instances crack initiation.
- Fatigue: Microstructures with finely dispersed RA and tempered martensite are formed by low RA content and fine austenite grain sizes, and tends to prevent nucleation of fatigue cracks, until very high stress levels are attained. However, fractures that occur at low cycles in low-stress applications are due to high RA content and the coarse nature of austenite grain sizes.
- Impact strength: Is defined as the measure of the ability of steel to resist fracture when subjected to a sharp blow. The austenite phase is not only very tough, but also posses higher impact strength than martensite phase. Increasing austenite content tends to increases the steels impact strength. Extra protection against cracking is achieved by higher impact strength, which prevents problems like spalling.

It is of paramount importance to establish equilibrium between the mechanical properties of a component and the optimum percentage of RA for any given application. See Figure 1.11.

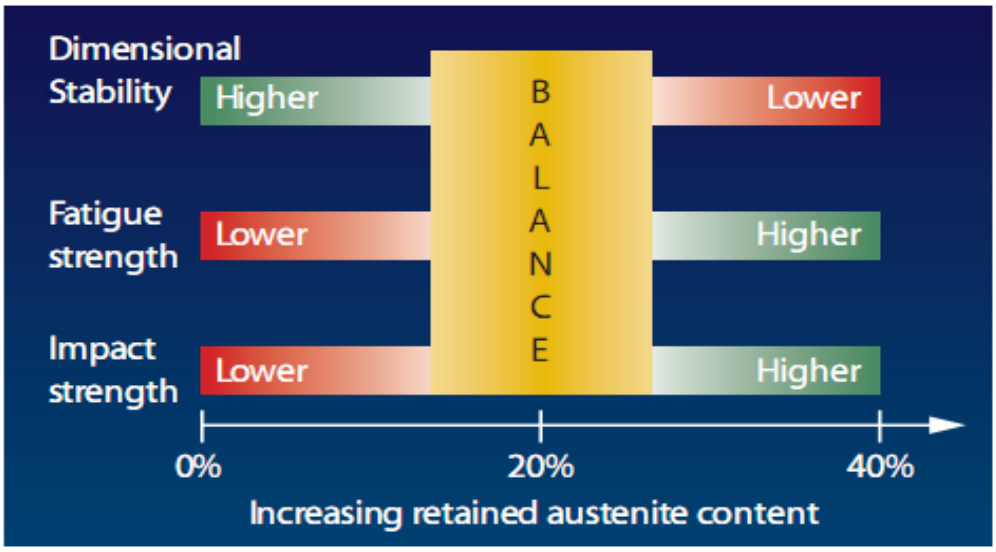

Figure 1.11: Balancing properties and RA content [40].

1.3.4 Industrial View Point of Retained Austenite

In tooling and die industrial application of steel component, they see RA as unwanted and undesirable. Premature failures are caused mostly by RA. The soft nature and low hardness of RA is also inconvenient with most applications that require the maximum attainable hardness to have high wear resistance properties.

Some percentage content of RA (5 to 30% determined by optical metallography, usually by comparison to known standards) is needed in bearing and gear industries for its application. Also, same mechanisms that affect tooling applications also affect gears, but there are some major differences. Gears are made of high impact strength case-hardened steel. Wear and fractures leads to failure of most tools, while many gear failures are the result of spalling in the tooth area. “Spalling is progressive macropitting that occurs when pits coalesce and form irregular craters, which cover a significant area of the tooth surface. Spalling occurs when the surface of a metal component is subjected to repeated cyclic loads. A crack forms and grows until a small portion of the surface breaks loose, damaging the surface and adding debris to the system” [40].

1.3.5 Percentage of Retained Austenite Reduction

Transformation of RA to martensite is done by tempering as an important method among other methods. The process requires holding for sufficient amount of time and temperature. To attain maximum transformation of this RA to martensite, two or more tempering is often executed. Apart from the tempering method, cold treatment at -85^{O}C (-120^{O}F) and cryogenic treatment at -195^{O}C (-320^{O}F) are other well known methods for this transformation. At lowered temperature the level of this transformation increases rapidly [55]. i.e., the percentage of RA is reduced.

The enhancing well-being of this RA is achieved by the ability to control the level of it without having miserable and disadvantageous effect of it when present in larger amount. Fatigue life, impact strength and dimensional stability are properties that many industries achieved by controlling the level of this RA, and more profit is made [55].

The desired equilibrium rate of RA is achieved by taking into account items like materials chemistry and heat treatment process variables such as steel chemistry, carbon content, austenitizing temperature, quenching rate and tempering temperature [55].

1.3.6 Retained Austenite Analysis

The hardening process of steels involves heating the steel sample to austenitization temperature which is relatively high temperature then quenching the steel samples with water, ice, oil or liquid nitrogen and followed by tempering process. When heating the steel sample, the room temperature phase stage of the steel is transformed into FCC structure that is austenite phase. This FCC structure austenite will further be transformed to fresh martensite by quenching process, and the fresh martensite is a hard, strong and brittle phase. Brittleness property of the steel is achieved by tempering process after the quenching process, and this brittleness is achieved by little (slight) loss in hardness. In real concept, some amount of austenite will be retained after quenching and tempering process hence causes materials performance debasement.

1.3.6.1 The Analysis Method

For analysis method, the austenite differs in crystal structure when compared with that of martensite and the other phases of steel such as the ferrite, bainite and pearlite. With these differences in crystal structure, the resultant diffraction pattern will also differ. Therefore, examining and compairing the peak of intensities in diffraction pattern from each of the phases approximate the amount of RA.

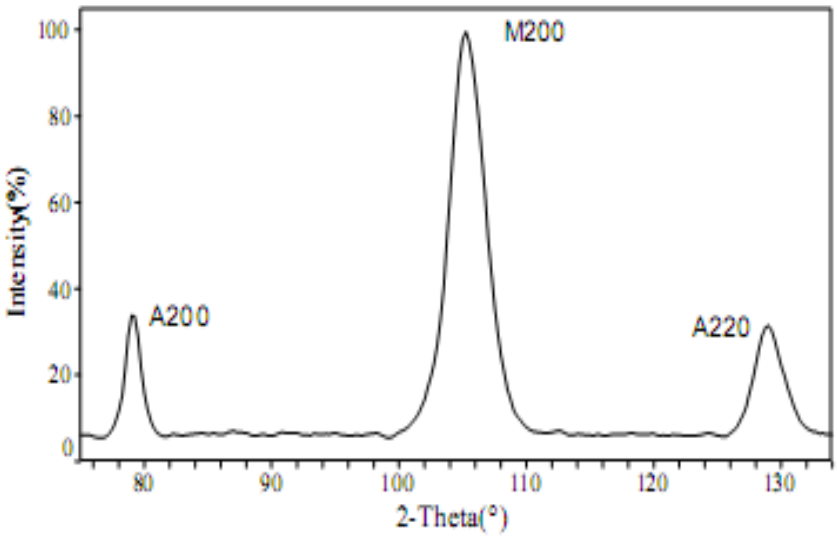

Figure 1.12: Diffraction pattern used for retained austenite analysis [55].

ASTM E975 and SAE SP-453 are the recently used standards for austenite measurements. An assumption is made to both standards that materials lack definite orientation and posses few amount of carbides. As illustrated in figure 1.12, it compares the M200 (200 martensite) intensity peak with the A200 and A220 (Austenite 200 and 220 peaks) respectively. For preferable orientation, comparison between the two intensities of austenite peaks is done with theoretical value of 1.475. For ratios in the range of 1.2 to 1.8, sample is carefully weighed to be free of preferred orientation.

To investigate the amounts of austenite and martensite, correlativity in differences between scattering power of the two phases, the intensity from the austenite must be multiplied by 0.572 (for 200 reflection) or 0.388 (for 220 reflection) to account for this discrepancy. In order to determine the relative amounts of the Austenite and Martensite, a

correlation must be made for the differences in scattering power of the two phases. For the above example in Figure 1.12, these intensities were found. For A200 peak the intensity was 2559, for M200 it is 23892 and for A220 it is 3869.

The calculated retained austenite in volume percent is computed as follows:

a) For Austenite 200 reflection.

Volume % = (2559×0.572) / (2559×0.572) + 23892 = 5.77%

b) Also using Austenite 220 reflection.

Volume % = (3869×0.388) / (3869×0.388) + 23892 = 5.91%

1.3.6.2 *Areas of Problem*

The RA analysis process is associated with likelihood of two states of difficulties. The initial came up when large amount of carbides that are not soluble are present, and the later happens when either any of the austenite or martensite has a preferred orientation.

Generally, it is very hard to rectify both difficulties using direct conventional methods, as mentioned in ASTM and SAE standards. Whole pattern method called Rietveld is, nowadays, the best method to solve these difficulties, and it involves analyzing the whole diffraction pattern alternatively for the other method which just analyzes the three peaks as shown in figure 1. 12.

The accuracy of ASTM/SAE methods are up to about 1% and 0.5% sensitivity level, where uncomplicated technique with carbides or preferred orientation are absent. In difficult and more complicated instances Rietveld method is mandatory; and same result is considered likely, despite in the presence of carbides and texture [55].

1.4 SUB-ZERO HEAT TREATMENT OF SAE 8620 STEEL

1.4.1 Cold Treatment for Transformation of Retained Austenite in SAE 8620 Steel

The heat treatment hardening processes of higher-alloy and carburized SAE 8620 steels are cold treated as an advanced technique to increase the hardenability of the steels.

The cold treatment process tends to transform the steel microstructure from soft and tough austenite to the hard, strong and brittle martensite phase and this cold treatment process occurs within the range of temperature of -70 to -120^{o}C (-90 to -190^{o}F). With high amount of transformation from austenite to martensite in SAE 8620 steel, it tends to increase the percentage of marteniste. Hence, SAE 8620 steel hardness increases. The wear resistance properties increases as hardness relates to wear resistance directly i.e increased hardness also increased the wear resistance properties (these wear resistance properties relates also to the amount of carbides present). For bearings and gears applications which needs some toughness to absorb impact strength and torsion loadings, some required percentage of RA is needed and paramount important in the steel microstructure.

1.4.1.1 *Describing the Heat Treatment Process*

The process of describing the heat treatment of SAE 8620 steel involves heating the steel to austenitizing temperature, then quenching or the rapid cooling. The process of heating to austenitizing temperature and followed by quenching hardens SAE 8620 steel. The last process involves tempering, and it involves heating to a temperature range less than that of austenitizing temperature and cold by air to reduces some hardness which increase the ductility properties of the steel. Basically, some applications required steel with good ductility ratio that relieve micro-stresses in the martensite matrix and this tends to prevent cracking.

1.4.1.2 *Increasing Hardness by Transforming Austenite to Martensite in SAE 8620 Steel*

At the M_s, austenite are transformed to martensite in SAE 8620 steel, and this M_s is specific for each type of steel depending on the steel composition. In most steels, this transformation is an isothermal process and move on perfectly as the temperature drops to the M_f. These temperatures, M_s and M_f, can be found on the steel specification sheets and heat treatment guides and standards, and are different for every alloy. Some amount of austenite, called RA, is often present after the hardenability process. In the presence of high contents of martensite and carbon percentages, it increases the hardness of steel as shown in Table 1.3. The carbon rate in weight percentage also affects the temperatures

where the martensite transformation begins (M_s) and is completed (M_f) as shown in Figure 1.13.

Table 1.3: Steel hardness at various martensite percentages for some low-alloy steel (Reprinted courtesy of ASM International) ASM handbook, heat treatment, Vol. 4, metals handbook 8th Ed., ASM International [56].

Rockwell C hardness (HRC) with martensite contents of:					
Carbon, %	50%	80%	90%	95%	99.9%
0.18	31	35	37.5	39	43
0.23	34	37.5	40.5	42	46
0.28	36.5	40.5	43	44.5	49
0.33	39	43.5	46.5	48.5	52
0.38	42	46	49	51	54
0.48	46.2	52	54	57	60

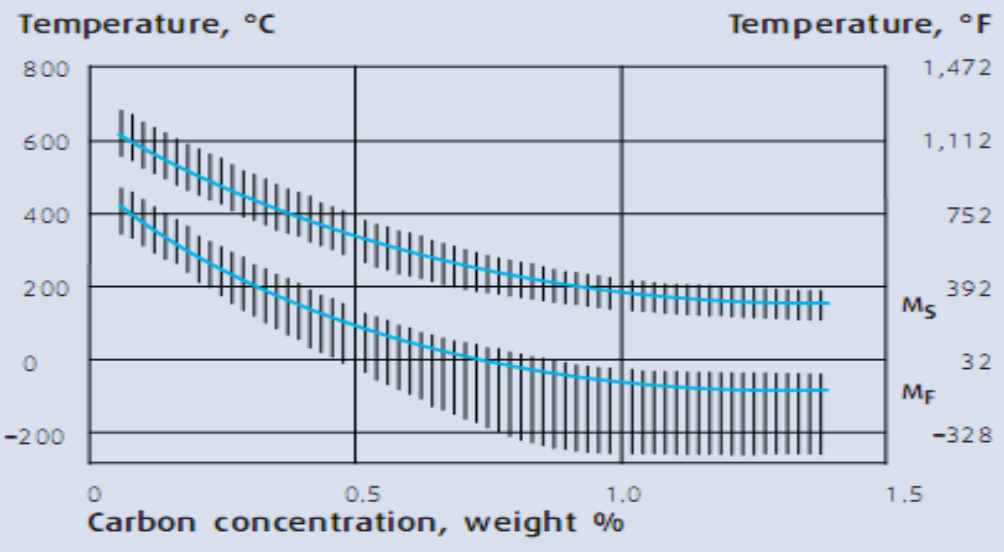

Figure 1.13: Effect of Carbon Content on M_s and M_f temperatures [57].

The martensite start and finish temperature plays an important role in the transformation process. Also, gran size affects these temperature. Increasing the grain size tend to lower the transformation temperatures. Therefore, high percentage of RA in SAE 8620 steel is found with higher austenitizing temperatures. Great transformation (austenite

to martensite) is achieved by cooling to sub-zero temperatures and hence increases the steels hardness and strength properties.

1.4.1.3 *Dimensional Stability Improvement*

At room temperature range, RA is not stable and gradually decay over time, therefore it does not have adverse effects for some applications. However, for applications with great and precise tolerance needed, the dacay process leads to dimensional changes as a result of variations in crystallographic sizes of the phases. Multiple cold treatment process cycles improves the dimensional stability of the steel.

1.4.1.4 *Cold Treatment Before and After Tempering*

To achieve the best and desired goal in the transformation process of RA to martensite, researchers prove that cold treatments of these steels should be done after quenching process but before the tempering process i.e. cold treatment in between the quenching and tempering process. Stabilization of RA is reported by many research findings. Figure 1.14 shows the sequential flows in order to achieve maximum percentage of transformation.

Figure 1.14: Heat treatment sequence for maximum transformation of austenite to martensite [57].

"Unfortunately, some alloys cannot tolerate a delay before tempering. The freshly formed untempered martensite is supersaturated with carbon, which makes it unstable, brittle and likely to crack. So from a commercial perspective, higher alloy steels are "snap tempered" at 100^{o}C (200^{o}F) to prevent cracking, then cold treated and tempered" [47].

1.4.1.5 *Applications of Cold Treatment*

Cold treatment has varieties of applications that improve the quality and performance of steels. Among the applications include carburization process of steels, in precision

component with precise tolerance, improving the hardness of steels, and also in bearings and gears applications.

1.4.2 Cryotreatment for Wear Resistance and Dimensional Stability

1.4.2.1 *Cryotreatment Introduction*

Mechanical properties of tool steels such as hardness, wear resistance, toughness, and dimensional stability have a property that can suffer an abrupt change to the performance of these tool steels. With the use of suitable sub-zero treatment, mechanical properties like wear resistance and tool life of high-alloy can be improved significantly [18-26, 58-61].

With correct usage of heat treatment and cryotreatment processes at liquid nitrogen temperature, the resulting properties are improved more than that of transformation from RA to martensite. Researchers did intensive experimental studies to find the effect of this cryotreatment and the reason behind the effect, but to have a good reason of this effect it requires modern and advanced analytical equipment.

Professor D. N. Collins carries out an intensive research on the effects of cryotreatment on tool steels at the University of Dublin. He states that: “In addition to the well-known effect of transforming RA to martensite, with the consequent increase in hardness, deep cryogenic treatment or cryotreatment has an effect on martensite. It causes crystallographic and micro structural changes which, on reheating, result in the precipitation of a finer distribution of carbides in the tempered microstructure, with consequent increase in both toughness and wear resistance” [60-61].

When cryogenic temperature decreases the amount of carbides precipitated increases. This phenomenon is shown in Figure 1.15 for D2 cold-work tool steel.

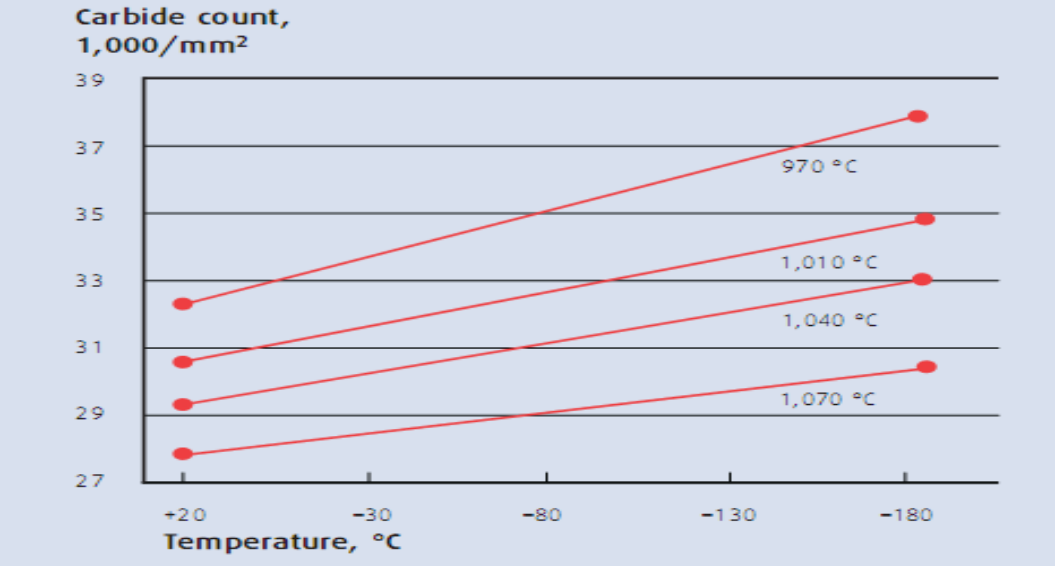

Figure 1.15: Effect of cooling to sub-zero temperature on carbide number for D2 steel. Austenitizing temperature of 970, 1010, 1040 and 1070°C were used before hardening process [61].

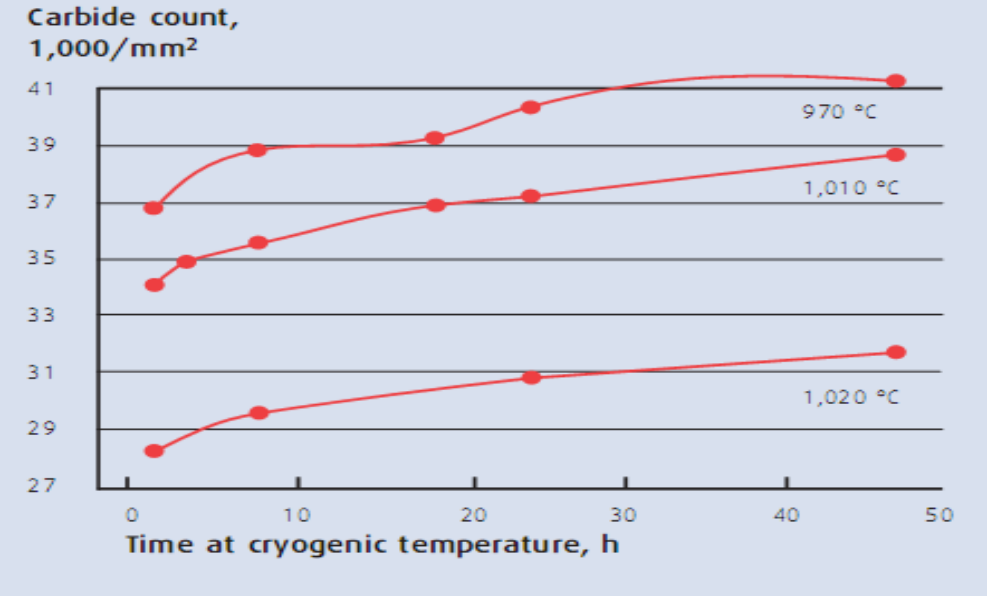

Figure 1.16: Effect of holding time at -196°C (-320°F) on carbide number for D2 steel. Carbides were measured using optical techniques [61].

As shown in Figure 1.17 [61]. The influence of holding time at temperature on hardness in Figure 1.17 illustrates that processing times in excess of 24 hours yield a higher hardness.

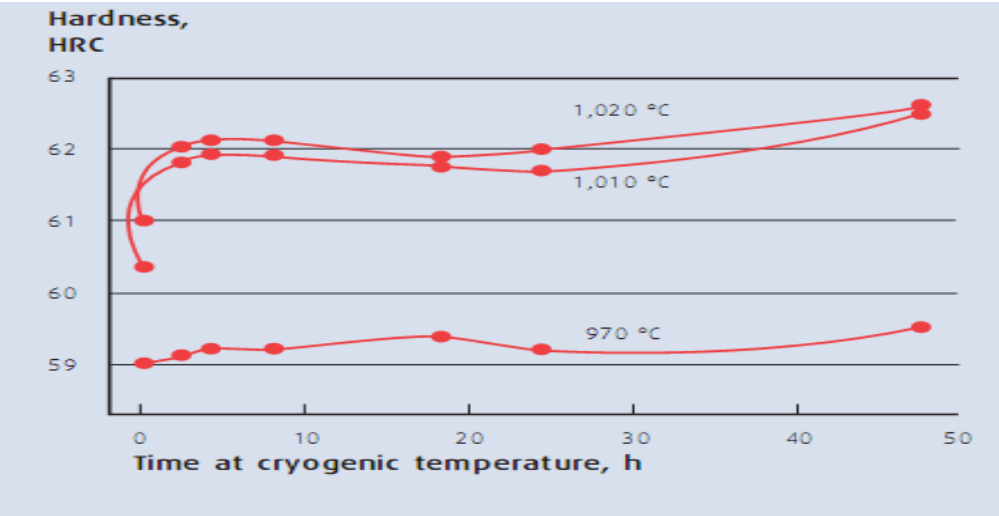

Figure 1.17: Effect of austenitizing temperature and holding time at cryogenic temperature on hardness of D2 cold-work tool steel [61].

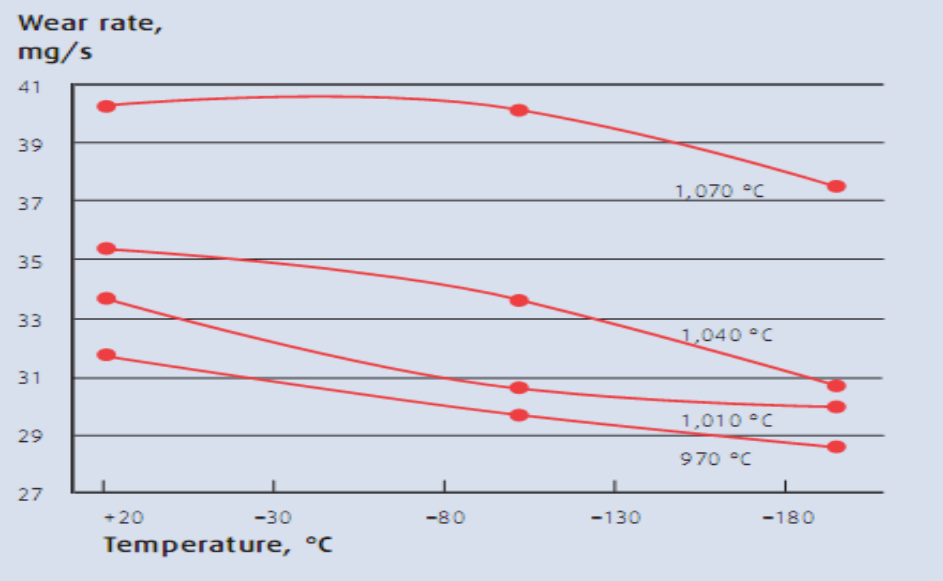

Figure 1.18: Influence of temperature on wear rate for D2 steel [61].

1.4.2.2 *Processing Cycles for Cryotreatment*

Information on Figure 1.16-1.18 clearly shows that lowest austenitizing temperature is used for hardened steels in order to achieve the optimum structure and also increases in wear resistance. "The cryoprocessing temperature should be ramped slowly by 2.5-5^{o}C/min (4.5-9^{o}F/min) [47]. For parts with thick cross-sections, it may be desirable to ramp down to an intermediate temperature and allow the temperature to become uniform before

continuing with the cool down. This procedure helps prevent cracking. Using gaseous nitrogen as the heat transfer medium allows close control of cool-down and warm-up rates [47]".

"Research shows that the deep cryogenic cycle should start with a slow cooling, continue with a fairly long soak (24 to 72 hours or more hours at temperature), and finally end with a slow warming to room temperature [18, 59, 60, 61]. The recommended heat-up process warms the material to room temperature at a rate of 1^{o}C/min in moving air [60].

1.4.2.3 *Successful Cryotreatment Applications*

Applications that prove to be successful in cryotreatment include cold-work tool steels, austenitic stainless steels, hot-work tool steels and high speed steels.

Researchers prove that cryotreatment responds well in cold-work tool steels, and these classes of steels are for tooling applications that operates below 200^{o}C (400^{o}F) like cold heading, blanking and trimming. The strength properties of austenitic stainless steels are greatly increased by cryogenic treatment of these steels. Hence, wear and corrosion resistance properties were obtained by foundaries for 300 and 400 series stainless steels used in oil pump applications [25].

1.4.2.4 *Unsuccessful Cryotreatment Applications*

The class of steels that transforms basically to bainite and also plain carbon steels do not improve in cryotreatment. But cast irons and ferritic stainless steels do not show any significant improvement.

CHAPTER 2

MATERIALS AND METHODS

This research work examines the relationship between microstructural characterizations, mechanical properties of SAE 8620 steel with different contents of boron in ppm rate. The objective of this research is to increase hardenability, wear resistance, dimensional stability and reducing production cost of the steel by adding boron.

Steel with elemental composition in weight percent of 0.15% C, 0.9% Cr, and 1% Mn and with the addition of 30 ppm of boron to this steel, shows a great increase in hardness up to 50% from the surface to a larger depth in the steel when compared to the same steel of indistinguishable composition without boron. Primarily, boron is added to steel to increase its hardenability and when its hardenability increases other mechanical properties like wear resistance and dimensional stability increase. It lowers transformation from austenite to ferrite and reduces production cost, this reduction in production cost typically for SAE steels when 30 ppm of boron is added it tends to substitute alloying element in weight percent of approximate amount of 0.5% C, 0.12% V, 1% Ni, 0.2% Mn, 0.4% Cr or 0.3% Mo which are more expensive and needed in much higher quantity [2].

2.1 MATERIALS

2.1.1 Properties of SAE 8620 Steel

The steel chosen for this research study was famous HSLA steel known as SAE 8620 steel with different boron contents used in bearings, automotive gearing, automotive body components and transmission components of cars applications. Furthermore, very little

research has been done on this SAE 8620 steel grade regarding the effect of boron addition in it. SAE 8620 was produced by melting at 1630^{O}C and then supplemented by boron, the casting process give rise to the steel sample with different ppm rate of boron and then rolled. The chemical analyses of the steel were done in TEST KIMYA LAB. 4460 program: G-COZLAB Bursa/Turkey. The chemical composition of the investigated steel sample is shown in table 2.1. The major alloying elements are Molybdenum (Mo), Chromium (Cr), Carbon (C), Nickel (Ni) and Boron (B).

Table 2.1: The chemical composition of SAE 8620 steel

Sample Code	**C**	**Si**	**Mn**	**Cr**	**Mo**	**Ni**	**B**	**Bsol**	**Binsol**
31	0.225	0.20	0.86	0.64	0.17	0.49	0.00033	0.00006	0.00041
32	0.223	0.19	0.83	0.63	0.16	0.49	0.00135	0.00091	0.00044
33	0.223	0.19	0.82	0.64	0.16	0.49	0.00296	0.00243	0.00053
34	0.226	0.17	0.79	0.63	0.16	0.49	0.00437	0.00356	0.00081
35	0.221	0.16	0.75	0.63	0.16	0.50	0.0058	0.00436	0.00134

The micro-alloying element is Boron (B) in ppm rate, and a designated pattern is used in numbering the steel which explains the boron content in the steel sample. A steel sample with code 31 contains 3.3 ppm of boron and will serve as the reference steel because hardenability begins with 8 ppm of boron [5]. Others include steel 32 with 13.5 ppm of boron, steel 33 with 29.6 ppm of boron, steel 34 with 43.7 ppm of boron and steel 35 with 58 ppm of boron. Table 2.2 shows the steel sample code with corresponding boron content in ppm rate and average hardness in HV. Table 2.3 shows the typical chemical composition of SAE 8620 steel without boron. Table 2.4 shows the mechanical properties of annealed SAE 8620 alloy steel without boron.

Table 2.2: Sample code with corresponding boron content.

Sample code	Boron content	Average HBN at 960^{O}C
31 steel	3.3 ppm	240.9 HBN
32 steel	13.5 ppm	262.4 HBN
33 steel	29.6 ppm	230.7 HBN
34 steel	43.7 ppm	223.4 HBN
35 steel	58 ppm	213.4 HBN

Table 2.3: The chemical composition of SAE 8620 Steel, in weight percent.

Element	Composition (wt. %)
C	0.18-0.23
Si	0.15-0.35
Mn	0.7-0.9
P	$\leq$ 0.035
S	$\leq$ 0.04
Cr	0.4-0.6
Ni	0.4-0.7
N	0.15-0.25

Table 2.4: Mechanical Properties of annealed SAE 8620 Alloy Steel without Boron [28].

Properties	Metric
Tensile Strength	530Mpa
Yield Strength	385Mpa
Elastic Modulus	190-210 GPa
Bulk Modulus (typical for steel)	140 GPa
Shear Modulus (typical for steel)	80 GPa
Poisson's Ratio	0.27-0.30
Hardness, Brinell	149
Hardness, Knoop (Converted from Brinell Hardness)	169
Hardness, Rockwell B (Converted from Brinell Hardness)	80

2.2 METHODS

2.2.1 Microstructural Examination

The chemical composition of investigated steel samples as-received is summarized in table 2.1 above. This composition is selected to obtain relatively high mechanical properties with low alloy contents and different boron contents. Metallographic methods in the study were conducted on the steel samples in as-received state and normalized states with different normalization temperatures from 860 to 1060^{O}C were carried out. The steel samples were heated with a PROTHERM FURNANCE MODEL: PLF 120/10 at various normalization temperatures of 860, 900, 960, 1010, and 1060^{O}C for different heating time and air cooled to atmospheric temperature. The steel samples were then grinded and polished mechanically with metkon^{R} FORCIPOL^{R} 2V GRINDER-POLISHER using different abrasive papers of sizes within the range of 120 to 1000. Furthermore, the samples were etched chemically with etching solution of 0.5 Nital, then the etched surface of the samples were dried with a dryer and samples microstructure were observed with an optical microscope with different magnifications to reveal the microstructural phases.

2.2.2 Heat Treatment

2.2.2.1 *Controlled Cooling*

One of the mechanisms to strengthen and harden most steels such as low-alloy, carbon and tool steels is heat treatment in which controlled amounts of martensite are produced in the microstructure. Heat treatment of steel begins with heating up the steel to austenitizing temperature. Austenite which is soft and tough phase is produced and this austenite is a stable phase according to the Fe_3C phase diagram over A_3 temperature. Next process involves cooling down to a suitable temperature depending upon the alloy content. The type of a heat treatment process to be done mostly depends on the desired microstructures and the steel composition considering the alloying elements. Additionally, subsequent cooling rate plays a great role in the resultant structure and properties [28].

The controlled cooling involves cutting the steel samples with a dimension of 6.5-7 mm in diameter and 3 mm in thickness, each sample was heated to austenitizing temperature of

960^{O}C and then controlled cooled with a cooling rate of 20^{O}C/min, 70^{O}C/min and 130^{O}C/min for 3.3 ppm, 13.5 ppm and 29.6 ppm of boron using the high temperature microscope stage that heat to a maximum of 1500^{O}C with a ceramic cup of dimension 7 mm in diameter and 3 mm in depth. For 31 steel samples with 3.3 ppm of boron, three sets of cooling rates of 20^{O}C/min, 70^{O}C/min and 130^{O}C/min are done. Additionally, controlled cooled treated at 20^{O}C/min, 70^{O}C/min and 130^{O}C/min were done for 32 and 33 steel samples each with 13.5 and 29.6 ppm of boron, respectively. Figure 2.1 shows the high temperature microscope stage used in the controlled cooling treatment process with a ceramic heating element made of Pt/Rh thermocouple (7/3 cup). To reduce the risk of decarburization, argon protective gas is supplied to the system and later microhardness of the samples was measured using a LECO M400-G2 micro hardness tester with a diamond indenter and load capacity within the range of 50 grams to 2 Kg. The measurements were made in terms of the Vickers hardness HV and also the microstructure images of the nine steel samples with different cooling rates.

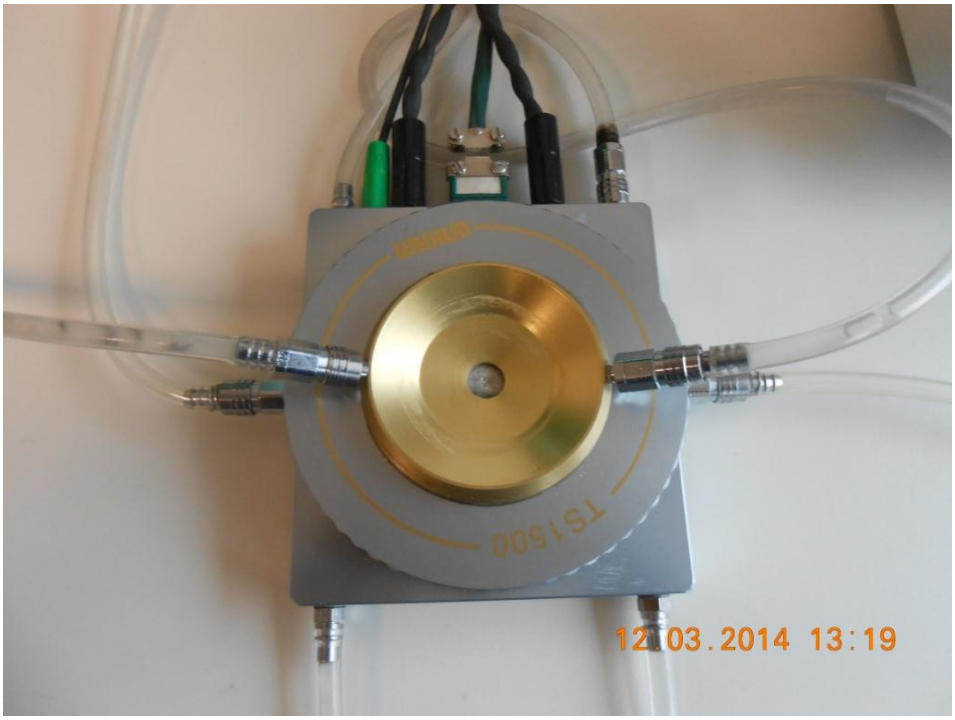

Figure 2.1: High Temperature Microscope Stage (with ceramic heating element made of Pt/Rh thermocouple 7/3 cup).

Figure 2.2: Controlled Cooling Process Experimental Set-up.

2.2.3 Mechanical Properties

2.2.3.1 *Hardness*

Hardenability is essentially the ease of forming martensite and reflects the ability of steel to be hardened to a specified depth [62, 63]. In a recent thermo-mechanical simulation studies [64, 65] it is stated that "the effectiveness of boron on hardenability have been found to be strongly dependent on soaking temperature and cooling condition, rather below a critical cooling rate boron has soften the low carbon aluminium killed steel".

For SAE 8620 steel, when heat treatment at different normalization temperatures develop a hard outer case with a soft and ductile core, the proportions of the alloying elements (Ni-Cr-Mo) are carefully controlled, with important qualities like extreme surface hardenability and good internal strength. The hardness measurements were done with UHT-900D Motorized Brinell Rockwell and Vickers Hardness Testers in both as-received state and normalized state with different normalization temperatures and 45 minutes heating time. The hardness machine was on the Brinell hardness scale HBN for all the heat-treated specimens with a conical diamond indenter of diameter (d) 2.5mm, test force (F) of

187.5 Kg and dwell time of 10 seconds. Three sets of readings are measured for each steel sample and then the average of the hardness of the sample is calculated.

2.2.3.2 *Wear Test*

Wear is the undesirable removal of material through various mechanical actions, and it is one of the most common causes of mechanical equipment failure. Materials may loss by such processes as abrasion, adhesion, erosion, corrosion and surface fatigue [66]. Wear test were done with a Nanovea Tribometer which offers precise and repeatable wear and friction testing using two standards of ISO and ASTM compliant Rotative and Linear modes. This device has a high resolution meaning data can be accurately recorded at specified interval of time or position. For the two set of modes, we use the Rotative mode (ASTM G99). The Rotative mode, which is the Pin-on-Disk, operates with the following principles: Steel samples were mounted with a polymer base on a mounting machine then placed flat and tight firmly. Ball made of Al_2O_3 with diameter of 6 mm was then loaded onto the steel sample with precisely variations in experimental weights of 5N, 10N and 15N and radius of 1.5 mm to make a circular wear track as the ball rotates on the steel sample. By measuring the deflection of the direct load cell, the friction coefficient is determined. For the Pin-on-disk process, wear rate are calculated from the volume of material lost during the test. Figure 2.3 shows the Nanovea Tribometer test machine to test the wear and friction properties of the steel samples.

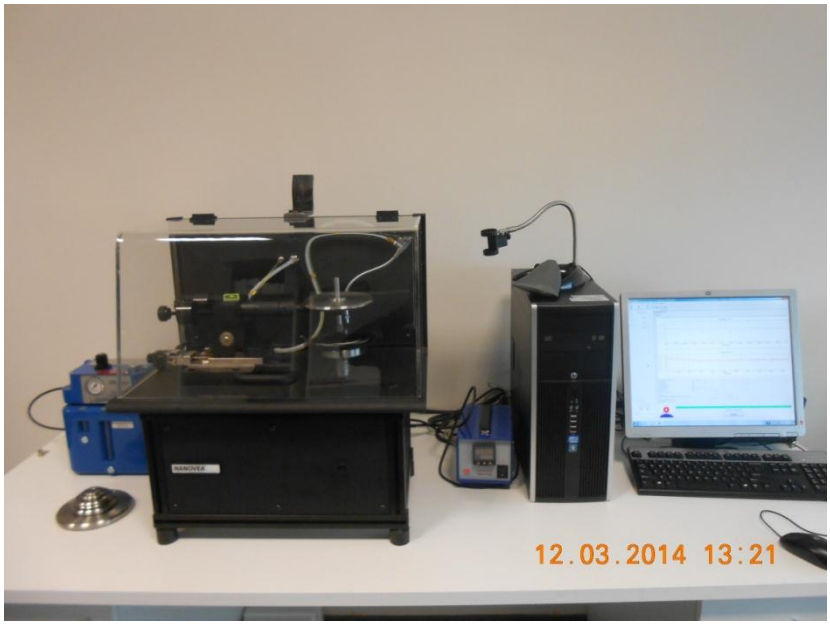

Figure 2.3: Nanovea Tribometer Test Machine Experimental Set-up.

With variations in test distances of 100m, 200m, 300m, 500m and sample speed of 3000mm/min. After each test the mass of the steel sample is measured to find the mass loss. Figure 2.4 shows the weight scale which has high precision and measures the mass loss after each wear test with sensitivity of 0.0001grams.

Figure 2.4: Weight scale with a sensitivity of 0.0001 grams

CHAPTER 3

RESULTS AND DISCUSSIONS

This chapter explains the experimental results described in chapter 2 and also discusses with references to the literature review in the introduction part of this write-up. In this research work, normalization process is done then the microstructural examinations of both the as-received and normalized states have been examined by using an optical microscope. Heat treatment process and the effect of mechanical properties on the studied steel, such as hardness and wear resistance properties were discussed. Conclusively, the chapter shows the results and discuss on the principles behind microstructures of heat treated in different conditions and as-received state, boron added steels. Additionally, mechanical properties such as hardness, mass loss for each wear test, wear rate and comparison between coefficient of friction with different content of boron have been investigated.

3.1 MICROSTRUCTURAL EXAMINATION

It is well known that most metallographic experimental research work performed depends on the surface condition of the samples. So in this research work, provisions and careful control techniques were adopted to avoid such variations in the specimen surface. Within the vicinity of this surface condition, some trial experiments were made especially during heat treatment of the steel samples in the furnace to control decarburization. In the controlled cooling experiment with high temperature microscope stage, argon gas is supplied to the system through the gas valve so decarburization had been kept minimum. Figure 3.1 shows the optical micrographs of as-received state of (a) 3.3 ppm and (b) 13.5 ppm (c) 29.6 ppm (d) 43.7 ppm (e) 58 ppm boron added steel samples.

The elongated and deformed grains are observed at the as-received state and it is clearly shown in the microstructure which is given in figure 3.1. Ferrite and pearlite structures are the general phases of the as received one. Optical micrographs of boron added steel samples show additional martensite besides ferrite and pearlite phases in the micro-structure. The boron steel samples with 3.3 ppm, 13.5 ppm, 29.6 ppm of boron show higher rates of martensitic structure and alpha-ferrite in fine grains form, but steel samples with 43.7 ppm and 58 ppm of boron are more of ferrite and pearlite other than martensite structures.

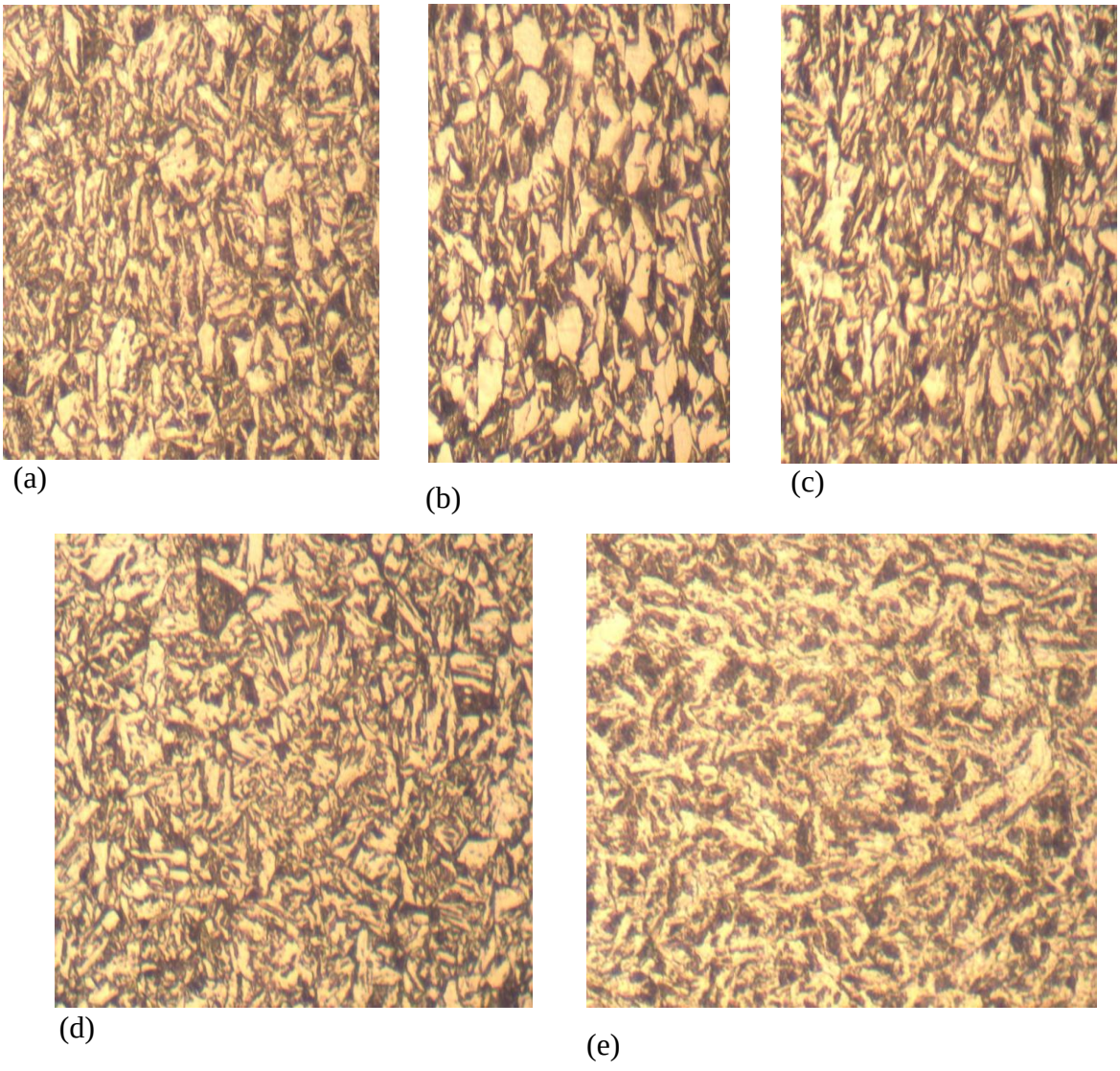

Figure 3.1: Optical micrographs of as-received state of (a) 3.3 ppm (b) 13.5 ppm (c) 29.6 ppm (d) 43.7 ppm (e) 58 ppm boron steel samples.

Normalization is used to refine the grains (i.e., to decrease the average grain size) and produce a more uniform and desirable size distribution of the grains. These fine grained pearlitic steels are tougher than coarse-grained ones and it is the main goal of normalization process. The microstructures of the normalized samples with different B contents were analyzed. The figures 3.2-7 show the typical optical micrographs of SAE 8620 steels with different boron content, normalization temperature and heating time. These micrographs illustrate how the microstructure affects with increasing boron content.

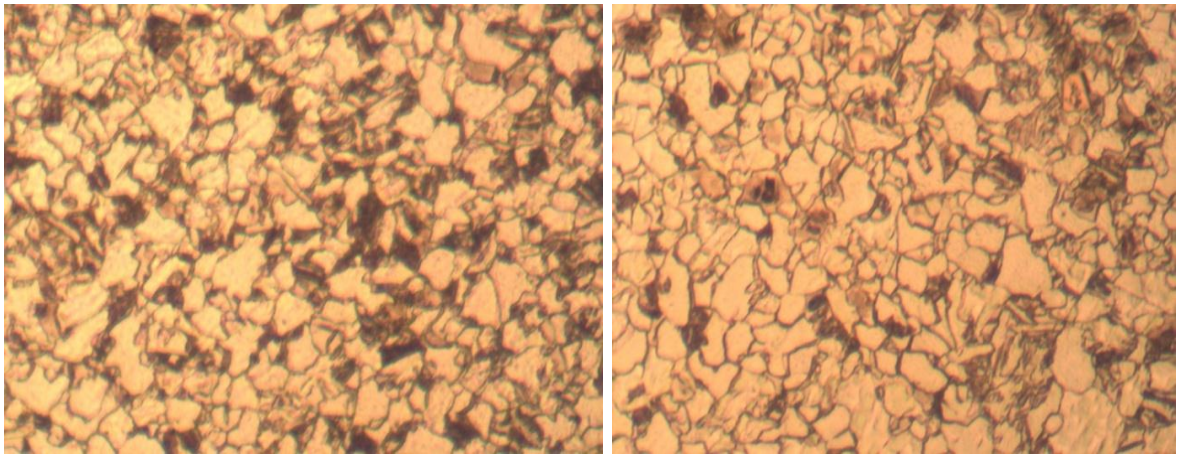

(a) (b)

Figure 3.2: Optical micrographs of SAE 8620 steel with 3.3 ppm of boron and normalization at 960^{O}C for (a) 45 minutes and (b) 60 minutes holding time.

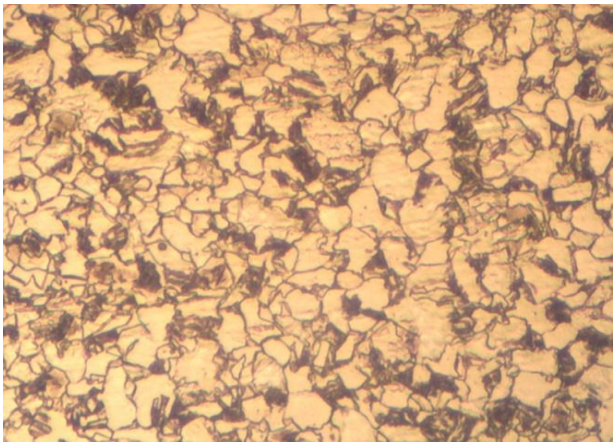

Figure 3.3: Optical micrographs of SAE 8620 steel with 3.3 ppm of boron 45 minutes holding time and normalization temperature of 1010^{O}C.

Boron added microstructure of SAE 8620 with 3.3 ppm shows ferrite, pearlite and martensite phases. Normalization temperature of 960^{O}C and different holding time show differences in the microstructure with that of 45 minutes having irregular orientation of ferrite compared to 60 minutes holding time. Additionally, more amount of martensitic phases are found with 45 minutes holding time at 960^{O}C normalization temperature and the normalized steel shows higher amount of transformation of austenite to martensite and hence more hardened structure. At an elevated normalization temperature of 1010^{O}C and 45 minutes holding time, easily identified martensite phase is observed.

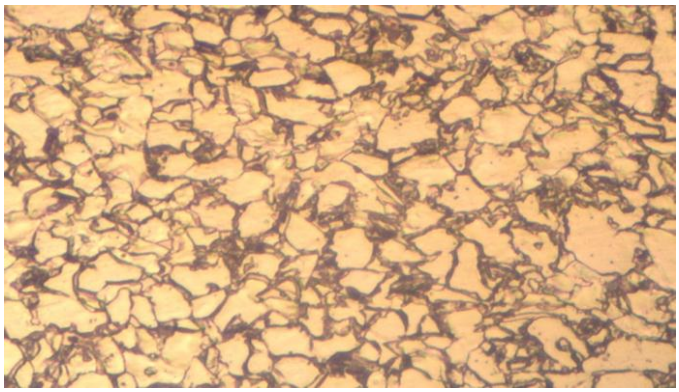

Figure 3.4: Optical micrographs of SAE 8620 steel with 13.5 ppm of boron 45 minutes heating time and normalization temperature of 1010^{O}C.

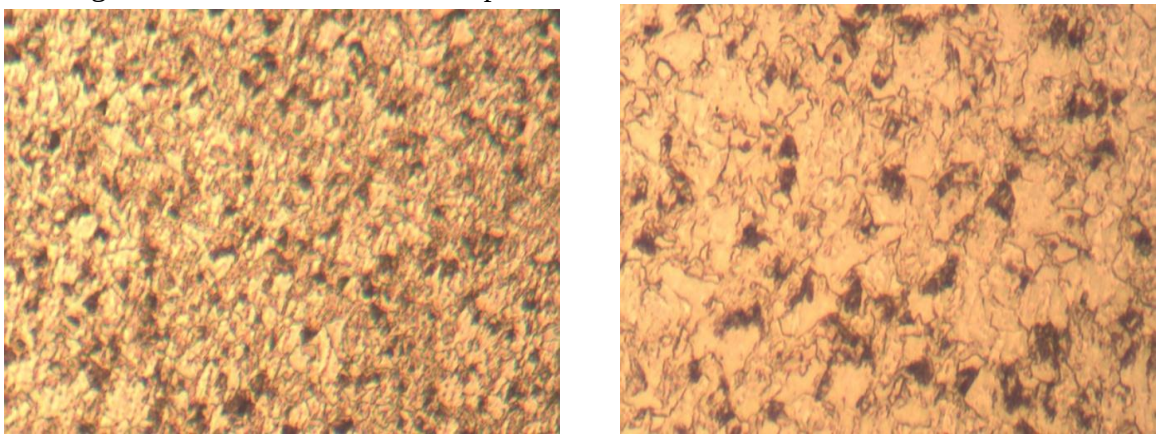

(a) (b)

Figure 3.5: Optical micrographs of SAE 8620 steel with 29.6 ppm of boron, normalization temperature of 960^{O}C and holding time of 60 minutes (a) 200× magnification (b) 400× magnification.

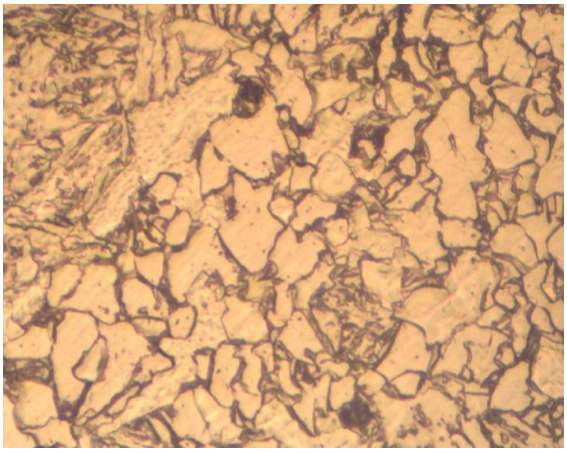

Figure 3.6: Optical micrographs of SAE 8620 steel with 29.6 ppm of boron, 45 minutes holding time and normalization temperature of 1010^{O}C.

Figure 3.6 shows the optical micrographs of SAE 8620 steel with 29.6 ppm of boron, ferrite are predominantly with larger grain-sizes. The martensites are closely concentrated in some regions compared to other regions. Figure 3.7(b) shows the presence of carbides and this is verified by comparing to literature, in a study of effect of austenitizing temperature on the microstructure of 15BCr30 and PL22 boron steels it clearly show the presence of iron-borocarbides $Fe_{23}(C,B)_6$ and the average size variations for the three austenitization conditions of 870°C, 1050°C and 1200°C and indicate that iron-borocarbides coalescence occurred at 870°C austenitization temperature. For the remaining two austenitization temperatures, iron-borocarbides solubilization and reprecipitation were observed. The austenitization temperature of 870°C lies below the $Fe_{23}(C,B)_6$ solubilization (965°C) [67],therefore avoiding boron segregation toward the grain boundaries [68]. However, the precipitate $Fe_{23}(C,B)_6$ coalesces and raises the grain boundaries interface energy, reducing the boron effect on steel hardenability.

Comparing the produced iron-borocarbides at 1050 and 1200°C, it can be seen that there is a larger precipitation/reprecipitation at grain boundaries for 1200 °C. This fact can be explained by the larger non-equilibrium segregation, which spurs the grain boundaries iron-borocarbide precipitation at bainite production temperature, during quenching cooling, reducing the steel hardenability.

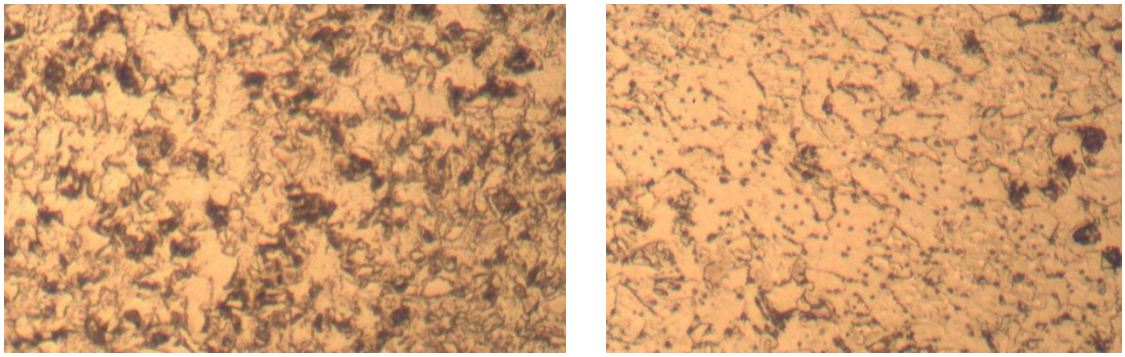

(a) (b)

Figure 3.7: Optical micrographs of SAE 8620 steel with 43.7 ppm of boron and normalization temperature of 960^{O}C (a) 45 minutes holding time (b) 60 minutes holding time.

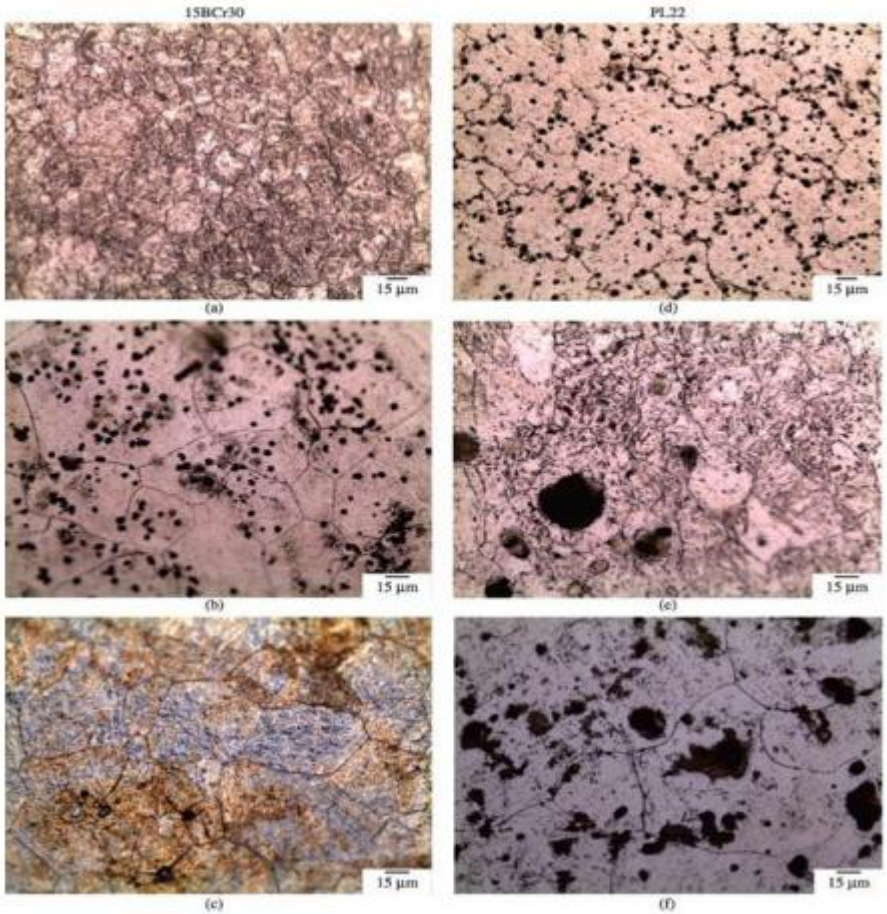

Figure 3.8: Variation of austenic grain sizes with respect to austenitization temperatures for 15BCr30 and PL22 steels: (a) and (d) 870^{O}C, (b) and (e) 1050^{O}C, (c) and (f) 1200^{O}C. [69].

3.2 HEAT TREATMENT

3.2.1 Controlled Cooling

The controlled cooling process will be explained in terms of the microstructural examination and the microhardness of the steel samples, then compared to the literature. As mentioned above (Chapter 1) fast cooling rate results in more transformation from austenite to martensite, and this FCC austenite is soft and tough while the BCC martensite is the hard, strong and brittle phase of the steel. This fact is shown and proved from cases of the microstructural examination and microhardness results, with the fastest cooling rate of 130^{O}C/min having predominantly martensite than subsequent lower cooling rates. Additionally, the microhardness value at the highest cooling rate is larger than the lower cooling rate values with a maximum of 295.9HV.

3.2.1.1 *Microstructural Examination*

Microstructural examination for controlled cooling process will be explained in terms of the 31, 32 and 33 steel samples each with different content of boron and different cooling rate of 20^{O}C/min, 70^{O}C/min and 130^{O}C/min. Figure 3.9 shows the microstructure images of 3.3 ppm of boron steel sample with 20^{O}C/min cooling rate.

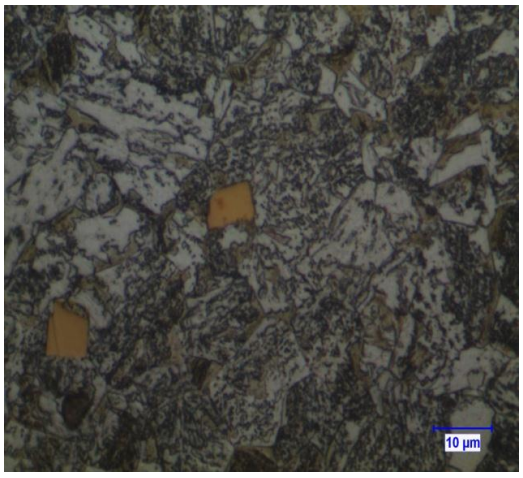

(a)

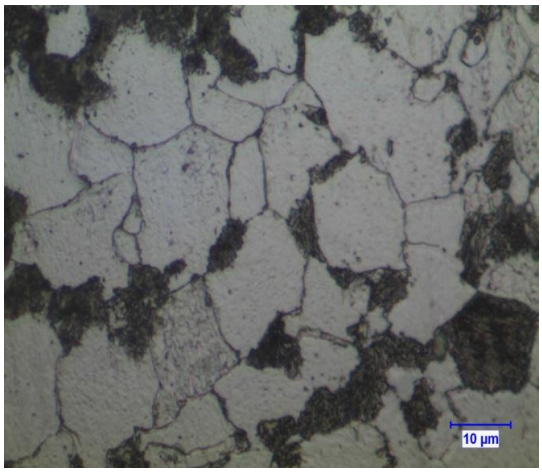

(b)

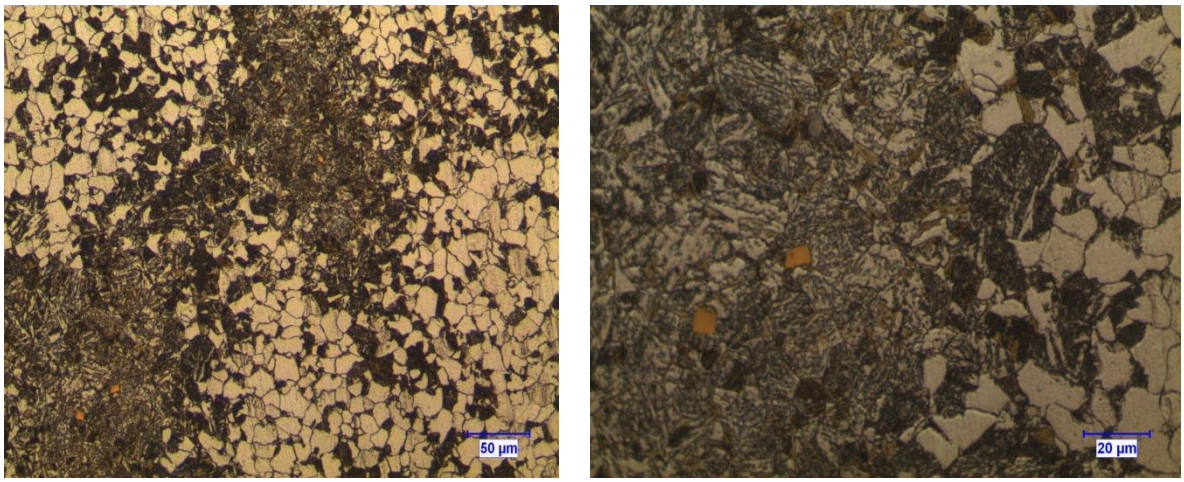

(c) (d)

Figure 3.9: Microstructure images of 3.3 ppm of boron (31 steel) steel sample with 20^{O}C/min cooling rate.

In figure 3.9(a), the microstructure shows the lath type martensite, Widmanstätten ferrite (white structure) and pearlite. Additionally, the polygonal titanium nitrite (TiN) inclusions have been observed [70]. It is shown that the grains are much smaller and lower in density. In figure 3.8 (b), ferrite grains are much bigger and equiaxed with the martensite having much density in some regions than other regions. Figure 3.9 (c) and (d) shows the presence of much TiN with (c) having oriented and sided ferrite.

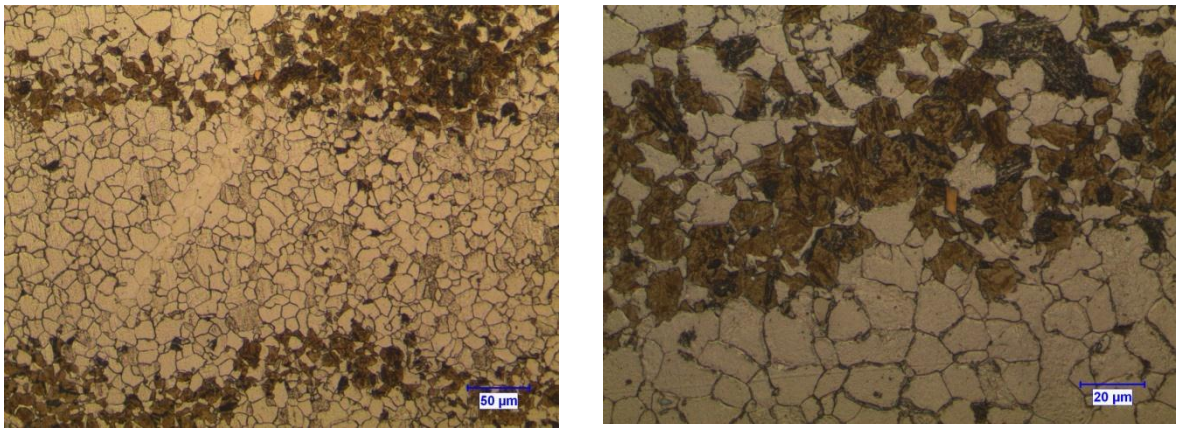

(a) (b)

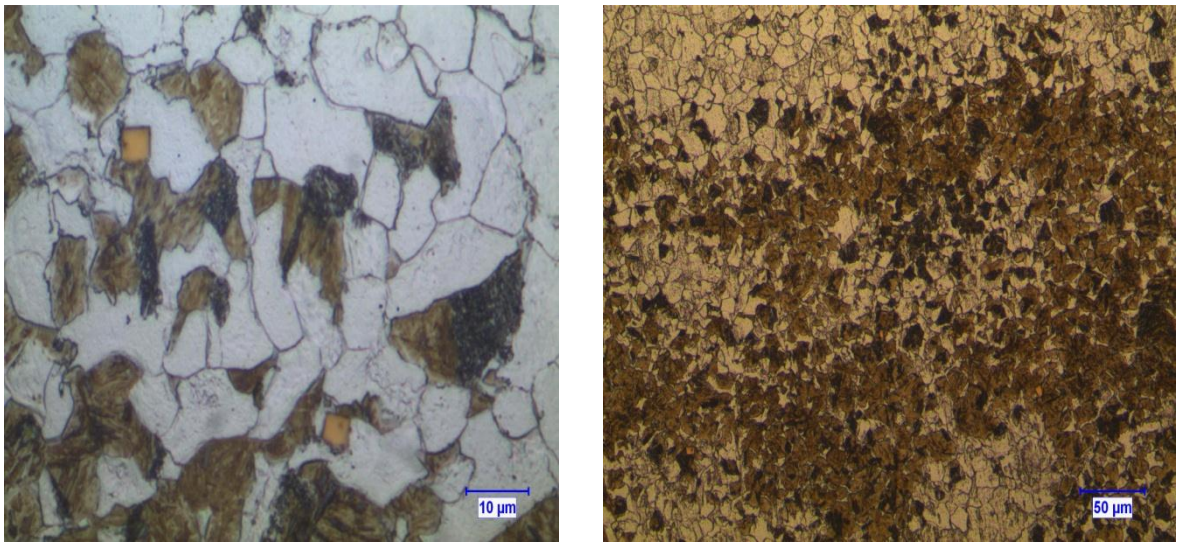

(c) (d)

Figure 3.10: Microstructure images of 3.3 ppm of boron (31 steel) steel sample with 70^{O}C/min cooling rate.

Figure 3.10 and figure 3.11 show the micrographs of 3.3 ppm of boron added SAE 8620 steel with an increment in the cooling rate to 70^{O}C/min and 130^{O}C/min. In figure 3.10 (a) the martensite and pearlite structures are observed in the structure with more amount of ferrite grains. Comparison between (a) and (d) shows that (d) has more amount of martensite and ferrite at the center of the micrograph image than ferrite. This difference reveals variation in the distribution of the phases in the microstructure. In figure 3.10 (c), the Widmanstätten ferrite appears as the white regions in different grain-sizes, also the lath type martensite and the pearlite are observed.

As can be seen in the microstructure of increased cooling rate more amount of martensitic structure is achieved.

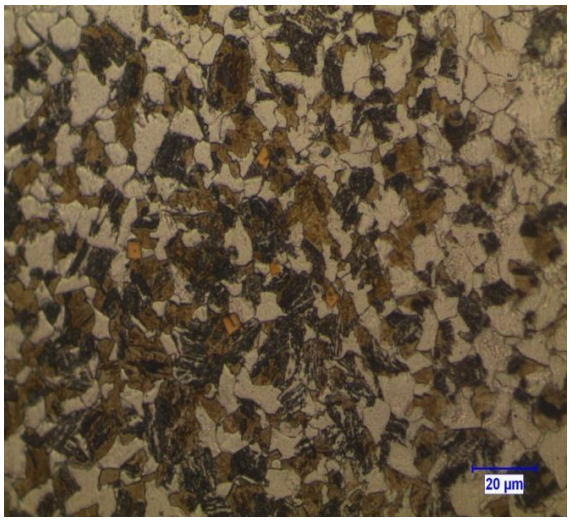

(a)

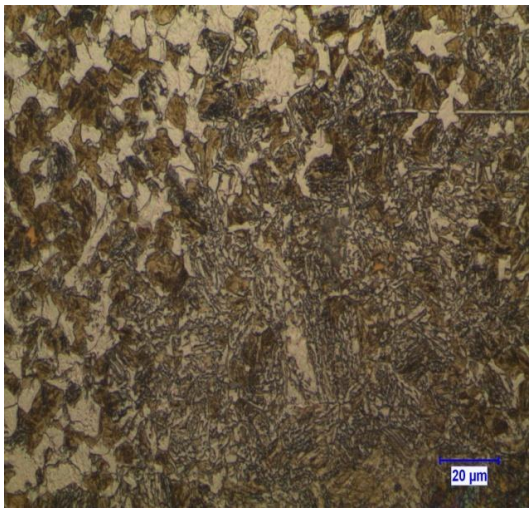

(b)

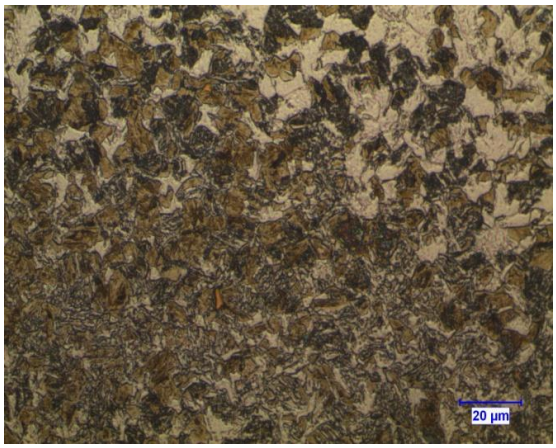

(c)

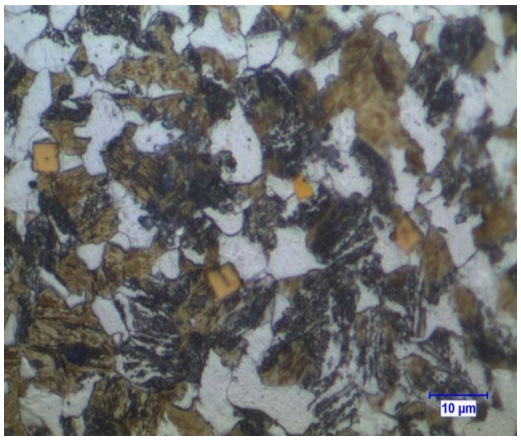

(d)

Figure 3.11: Microstructure images of 3.3 ppm of boron (31 steel) steel sample with 130^{O}C/min cooling rate.

The microstructure images for 130^{O}C/min cooling rate is predominantly of martensite structure which shows more amount of transformation, and proves the existence of lath type martensite and Widmanstätten ferrite. Smaller grains are observed as compared to 20^{O}C/min and 70^{O}C/min cooling rate.

Steel samples with 13.5 ppm of boron show increase in hardness. And this is due to increase in boron content and more amount of martensitic transformation as compared to the steel sample with 3.3 ppm of boron when controlled cooled under same conditions. Variations in argon supply to the 20^{O}C/min and 70^{O}C/min cooling rate are done

intentionally to minimize also the rate of decarburization. And the result shows the effect of this variation in the supply of the gas. Figure 3.12, 3.13, 3.14 shows microstructure images of 13.5 ppm of boron (32 steel) steel sample with 20^{O}C/min, 70^{O}C/min and 130^{O}C/min cooling rate respectively.

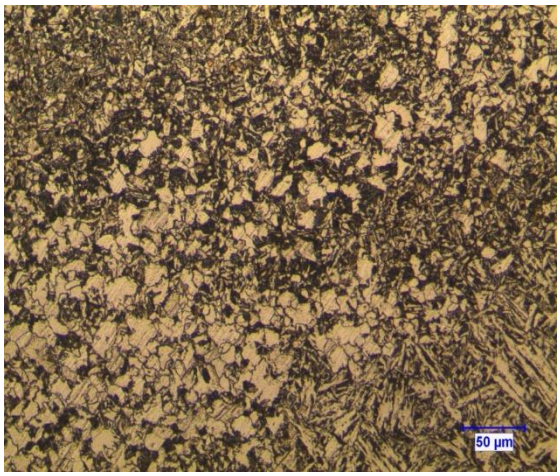

(a)

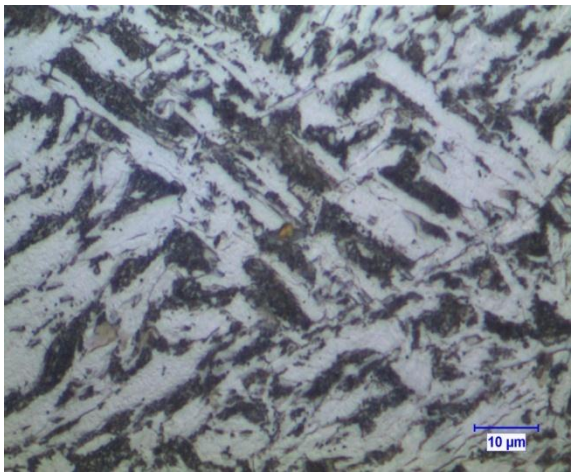

(b)

Figure 3.12: Microstructure images of 13.5 ppm of boron (32 steel) steel sample with 20^{O}C/min.

(a)

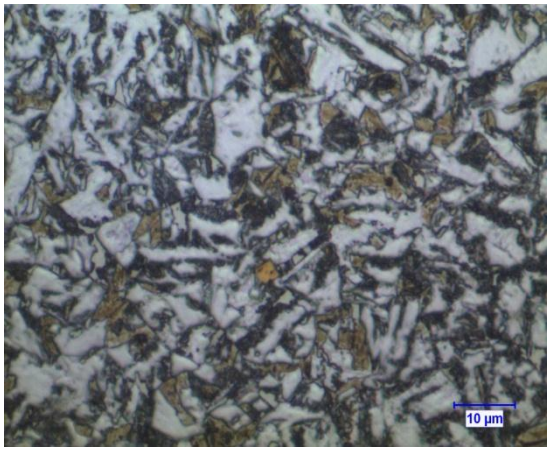

(b)

Figure 3.13: Microstructure images of 13.5 ppm of boron (32 steel) steel sample with 70^{O}C/min.

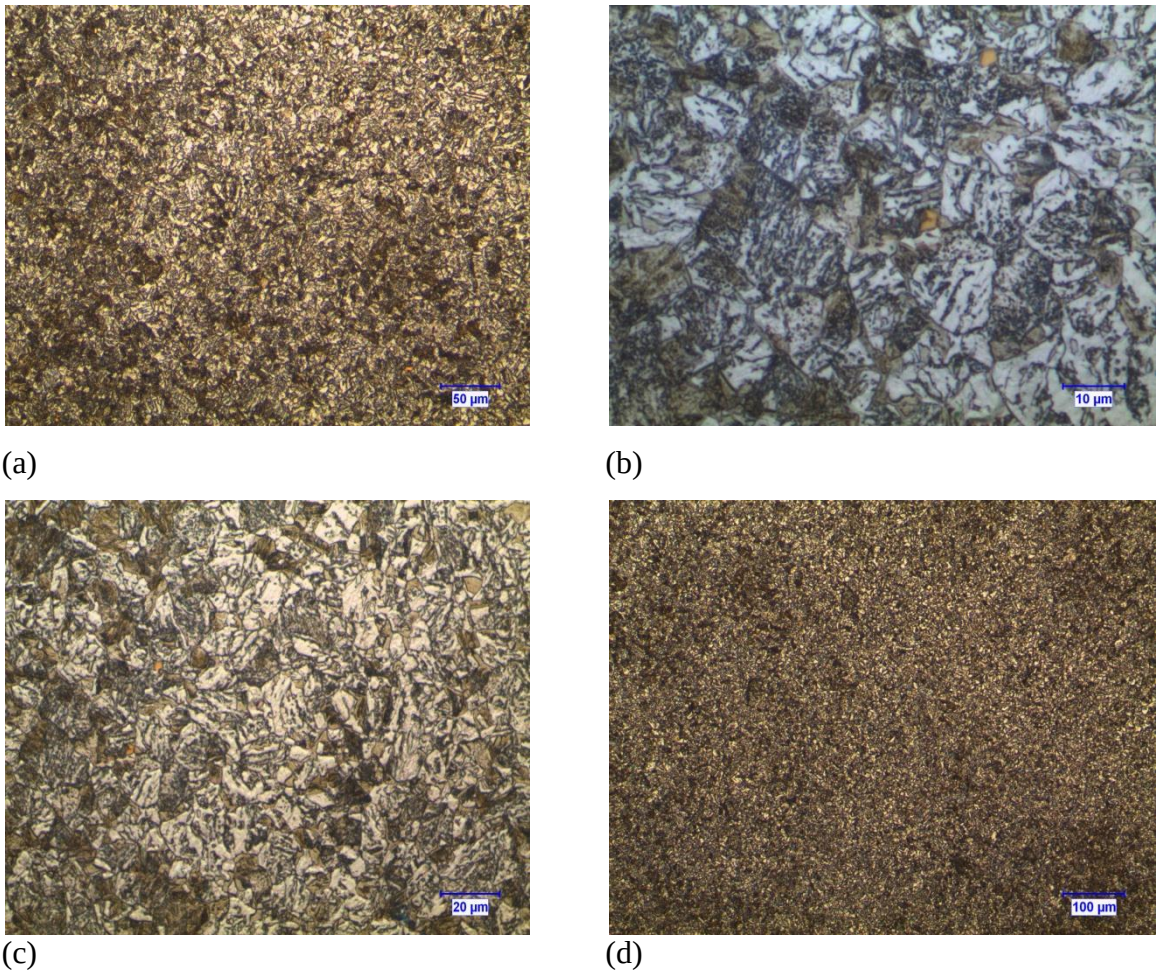

(a) (b)

(c) (d)

Figure 3.14: Microstructure images of 13.5 ppm of boron (32 steel) steel sample with 130^{O}C/min.

For steel samples with 29.6 ppm of boron (33 steel), lath type martensite, Widmanstätten ferrite and pearlite are shown in the microstructure. The presence of more amount martensitic structure tallies with the cooling rate as much martensitic structure is attained with 130^{O}C/min cooling rate. Figure 3.15, 3.16, 3.17 shows microstructural images of 29.6 ppm of boron (33 steel) steel sample with 20^{O}C/min, 70^{O}C/min and 130^{O}C/min cooling rate respectively.

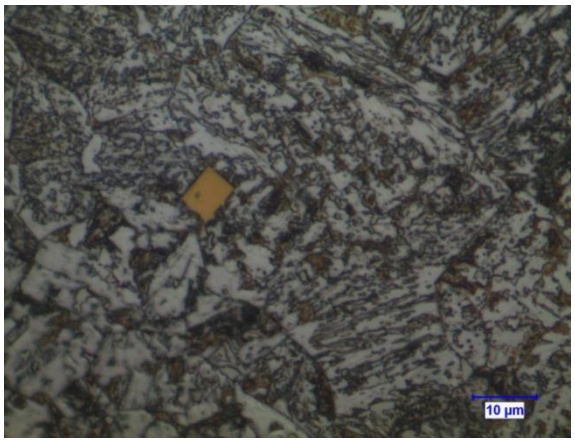

(a)

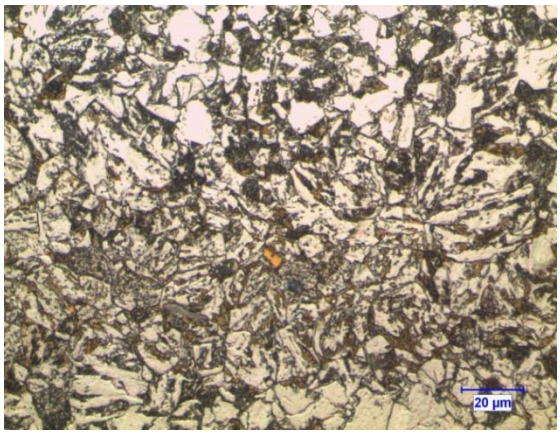

(b)

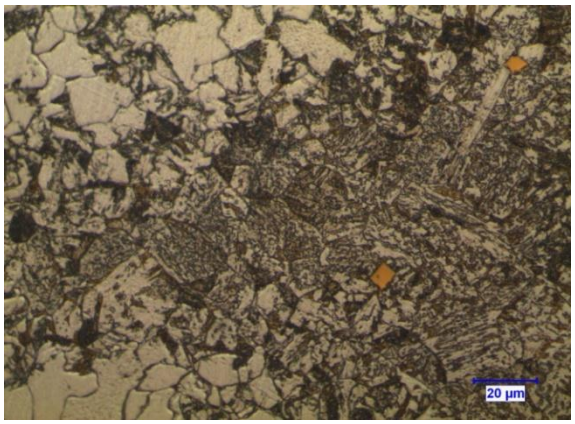

(c)

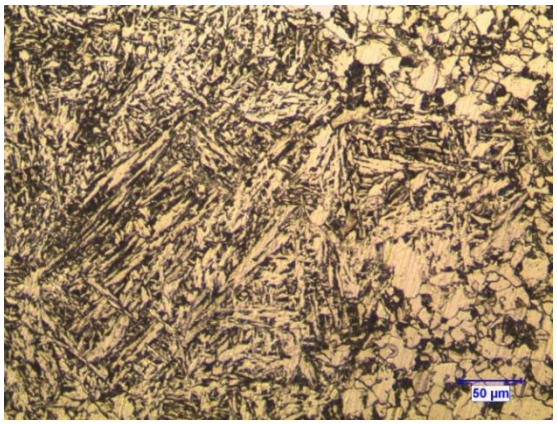

(d)

Figure 3.15: Microstructure images of 29.6 ppm of boron (33 steel) steel sample with 20^{O}C/min cooling rate.

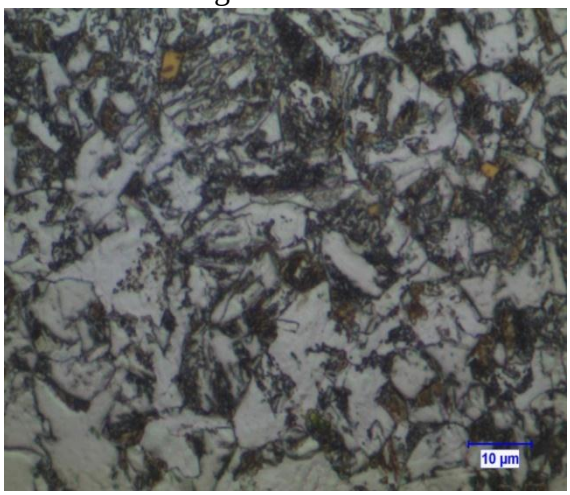

(a)

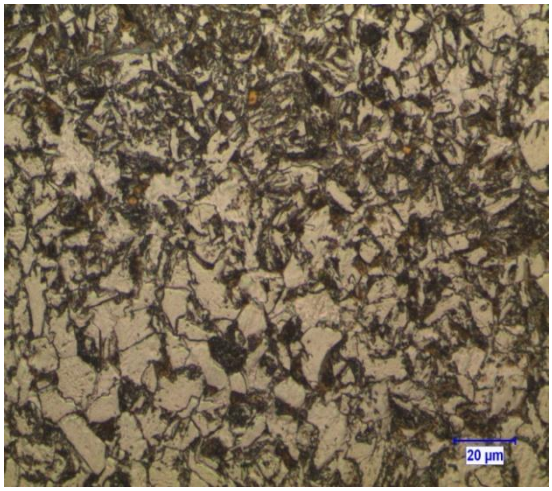

(b)

Figure 3.16: Microstructure images of 29.6 ppm of boron (33 steel) steel sample with 70^{O}C/min cooling rate.

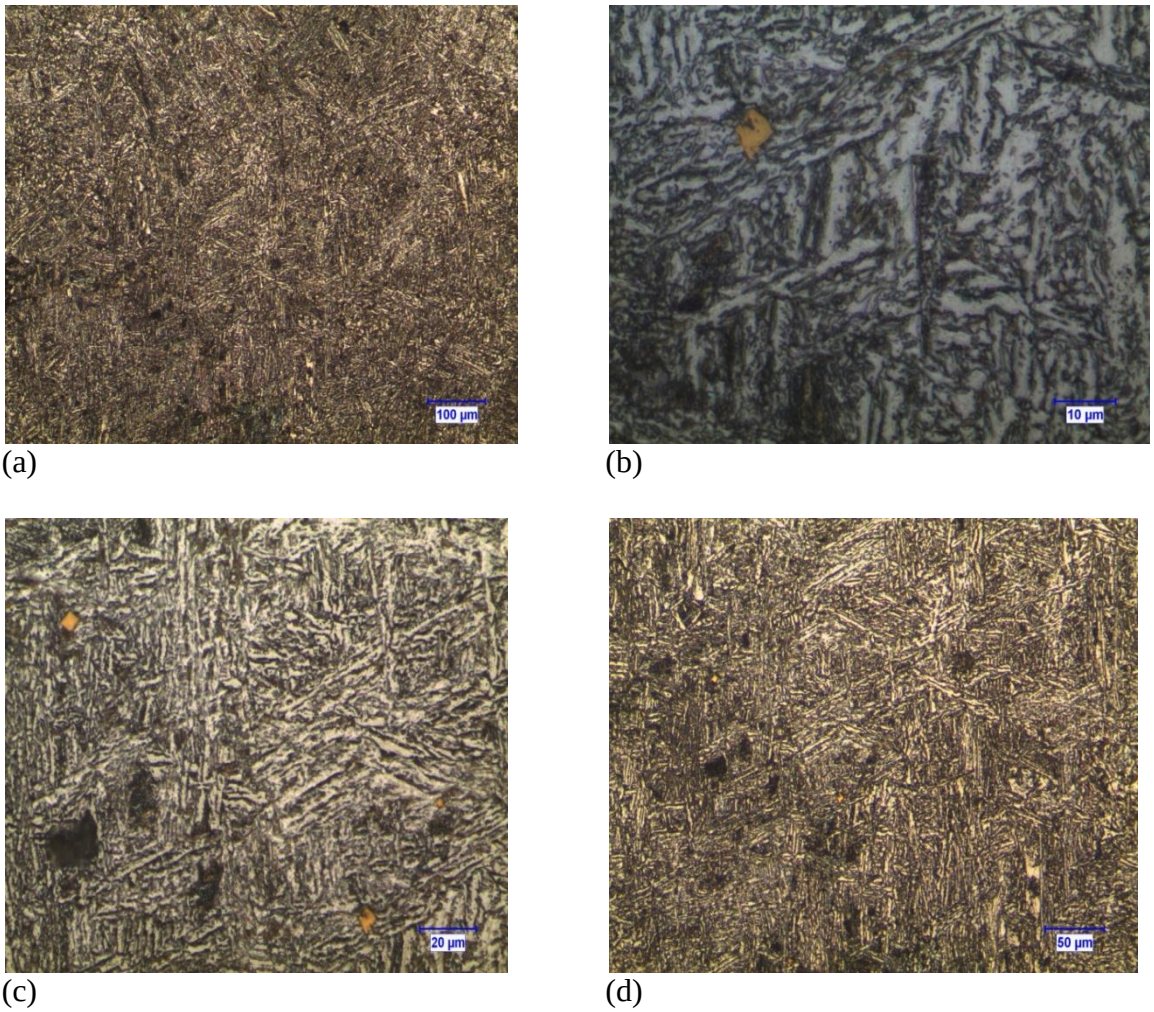

(a) (b)

(c) (d)

Figure 3.17: Microstructure images of 29.6 ppm of boron (33 steel) steel sample with 130^{O}C/min cooling rate.

It is clearly seen from the microstructure images that samples with cooling rate of 130^{O}C/min have more martensitic structure hence more hardened.

3.2.1.2 *Hardness*

Steel sample with 3.3 ppm of boron, the cooling rate of 130^{O}C/min has Vickers Hardness of 238.4 HV which is higher than that of 70^{O}C/min and 20^{O}C/min with 171.9 HV and 162.0 HV, respectively. This is clearly shown from literature that fast cooling result in more transformation from austenite to martensite (hard and strong phase) and also the microstructure shows higher percentage of martensite with the 130^{O}C/min cooling rate, than 70^{O}C/min and 20^{O}C/min respectively.

For steel samples with 13.5 ppm of boron (32 steel), the average Vickers microhardness HV of 130^{O}C/min, 70^{O}C/min and 20^{O}C/min cooling rates are 316.0 HV, 274.0 HV and 279.6 HV, respectively. The microstructures revealed that steel sample with fast cooling rate (130^{O}C/min) has predominantly martensite structure hence more hardened as proved from measured Vickers Hardness. Additionally, when performing the experiment for the 70^{O}C/min and 20^{O}C/min there is variation in supply of argon protective gas. This variation clearly shows in hardness with 20^{O}C/min cooling rate having more Vickers microhardness of 5.6 HV than 70^{O}C/min, and this happen as a result of decarburization in steel sample with 70^{O}C/min cooling rate. Table 3.1 shows the three sets of Vickers microhardness of each steel sample and corresponding cooling rate.

Furthermore, steel samples, with 29.6 ppm of boron (33 steel) and the average Vickers microhardness HV of 130^{O}C/min, 70^{O}C/min and 20^{O}C/min cooling rates are 295.9 HV, 291.5 HV and 246.7 HV, respectively. It also shows higher hardness with the fast cooling rate (130^{O}C/min) process and its microstructure with predominant martensite phase. Conclusively, steel samples with 130^{O}C/min cooling rate have the highest Vickers microhardness as a result of greater transformation from austenite to martensite and is clearly shown by the optical micrographs. Table 3.2 shows the average Vickers microhardness and the corresponding cooling rates.

Table 3.1: The three sets of Vickers microhardness of each steel sample and corresponding cooling rates.

Sample code	**31**			**32**			**33**		
Cooling rate (^{O}C/min)	**20**	**70**	**130**	**20**	**70**	**130**	**20**	**70**	**130**
Vickers microhardness (HV)	141.1	147.2	202.3	308.7	262.8	270.6	274..8	286.0	284.7
	184.7	195.5	226.8	292.8	240.9	308.0	229.5	242.8	305.2
	160.2	173.1	286.0	237.3	318.4	369.3	235.8	345.6	297.8
Average	162.0	171.9	238.4	279.6	274.0	316.0	246.7	291.5	295.9

Table 3.2: The average Vickers microhardness and the corresponding cooling rates.

Average Vickers Microhardness (HV)			
Cooling rate	**31**	**32**	**33**
20^{O}C/min	162.0	279.6	246.7
70^{O}C/min	171.9	274.0	291.5
130^{O}C/min	238.4	316.0	295.9

Figure 3.18 shows the average Vickers microhardness plotted against the cooling rates for 3.3 ppm, 13.5 ppm and 29.6 ppm of boron. It can be seen from the graph that increase in microhardness is achieved by increasing the cooling rate from 20^{O}C/min to 130^{O}C/min. But for 32 steel sample, between 20^{O}C/min and 70^{O}C/min cooling rate, a drop of 5.6 HV is shown due to minimal supply of argon protective gas.

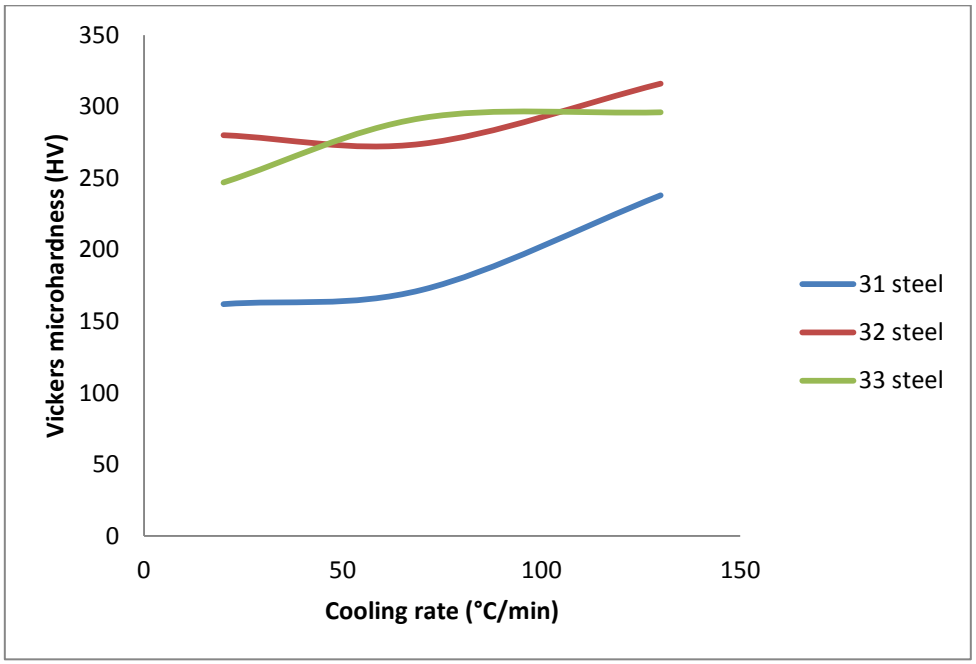

Figure 3.18: Graph of Vickers microhardness (HV) against cooling rate (^{O}C/min) for 3.3 ppm, 13.5 ppm and 29.6 ppm of boron.

3.3 MECHANICAL PROPERTIES

3.3.1 Hardness

Table 3.3 shows the average Brinell Hardness Number (HBN) results at various normalization temperatures measured with UHT-900D Motorized Brinell Rockwell and Vickers Hardness Testers. The average is found by taking three readings of the hardness and then calculating its average.

Table 3.3: Average Brinell Hardness Number (HBN) results of SAE 8620 steels at various normalization temperatures and 45 minutes as heating time.

As received	Temp.	31 Steel	32 Steel	33 Steel	34 Steel	35 Steel
237.3HBN	**860^{O}C**	221.3HBN	228.4HBN	238.3HBN	237.6HBN	239.9HBN
229.7HBN	**900^{O}C**	219.3HBN	230.3HBN	241.8HBN	242.8HBN	226.0HBN
249.7HBN	**960^{O}C**	240.9HBN	262.4HBN	230.7HBN	223.4HBN	213.4HBN
245.1HBN	**1010^{O}C**	193.4HBN	222.4HBN	211.9HBN	208.2HBN	201.0HBN
244.0HBN	**1060^{O}C**	205.5HBN	207.5HBN	218.6HBN	211.2HBN	201.5HBN

The maximum hardness was 262.4HBN for the 13.5 ppm of boron steel sample at normalization temperature of 960^{O}C, but as-received state it has a hardness of 229.7HBN and it is low compared to other steel samples with various boron contents, with difference of 14.3 HBN from the highest hardness for the as-received state. This maximum hardenability obtained when compared to amount of soluble boron shows that the content of the dissolved boron did not exceed that needed for the decrease of the boundaries energy in regions with ferrite formations, and also normalization at higher temperature with low carbon content shows lower hardness. Figure 3.19 shows a drastic increase in hardness with 13.5 ppm and 3.3 ppm of boron samples but with best hardness in the 13.5 ppm of boron sample (262.4 HBN). The 29.6 ppm of boron at 860^{O}C it hardness was 238.3HBN which slightly increase to 241.8HBN at 900^{O}C but decrease to 230.7HBN at elevated temperature of 960^{O}C. The steel samples with 43.7 and 58 ppm of boron tends to decrease in hardness from the temperature range of 860^{O}C and 960^{O}C.

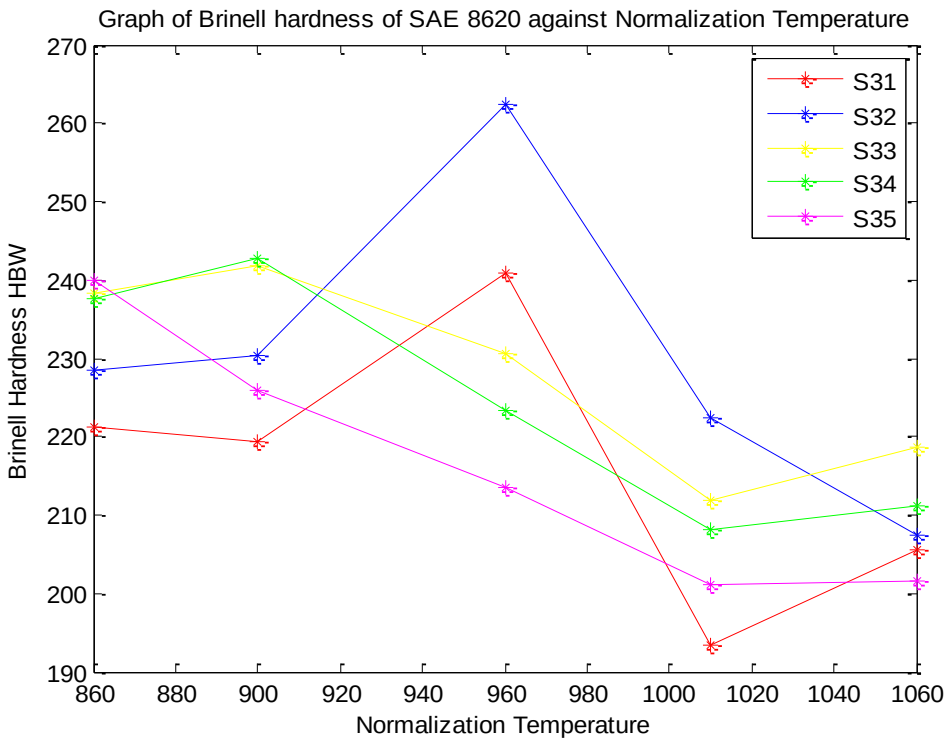

Figure 3.19: Graph of Brinell hardness (HBN) of SAE 8620 steels against normalization temperatures of 860^{O}C, 900^{O}C, 960^{O}C, 1010^{O}C and 1060^{O}C.

Also, from the figure it shows drastic decrease in hardness for the 3.3 ppm and 13.5ppm boron steel sample for an increase in normalization temperature of the process from 960^{O}C to 1060^{O}C. Despite the difference in the amount of boron but only 2 HBN were measured from the average hardness of 3.3 ppm and 13.5 ppm, this clearly indicates normalization temperature has a great influence on the hardness and must be correctly applied not to destroy the effect of the microalloying element boron in the hardness process. Consequently, for 29.6 ppm, 43.7 ppm and 58 ppm at elevated temperature shows slight and uniform decrease in hardness. Figure 3.19 shows the graph of Brinell hardness against boron content for different normalization temperature.

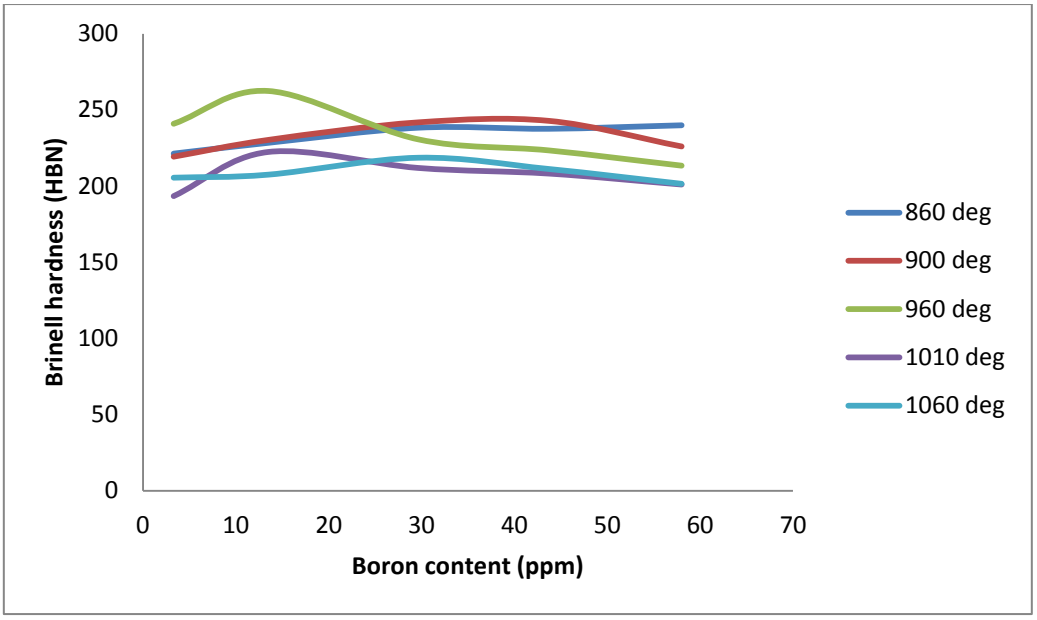

Figure 3.20: Graph of Brinell hardness against Boron content.

3.3.2 Wear Test

3.3.2.1 *Mass Loss for each test*

For as-received state of the steel samples, wear test with normal force (F_N) of 5N and test distance of 100m, 200m and 300m were done. Table 3.4 shows the mass loss (Kg) after each test and corresponding sliding distance for the as-received state of the steel samples.

Table 3.4: Mass loss (Kg) after each test for the as-received state of steel samples.

Sliding Distance (m)	Mass loss (kg) after each test		
	31	32	33
100	0.000002	0.0000011	0.0000076
200	0.0000045	0.0000037	0.0000089
300	0.0000086	0.0000075	0.0000118

The mass of the sample decrease after each test as a result of abrasive wear of the surface of the sample. This decrease in mass is also shown in literature, and will be seen clearly from the plots of graph of mass loss against distance in figure 3.21 for 31, 32 and 33 steel samples respectively. At the initial state, plots of the graph show uniform increase in the mass loss against the sliding distance. Within 200m sliding distance a variation in the mass loss appears as bends which show non uniform decrease in the mass loss at that

region of the steel sample and further maintain this uniformity within sliding distance up to the maximum sliding distance of 300m within the vicinity of our experiment.

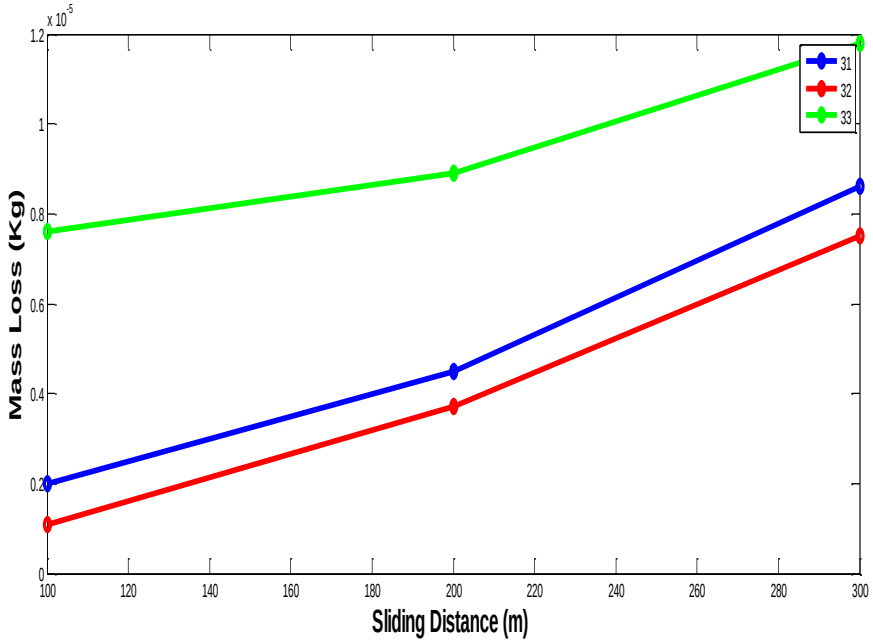

Figure 3.21: Graphs of mass loss (Kg) against sliding distance for each test for the as-received state and normal force of 5N.

For 31 steel sample, a normalization temperature of 960^{O}C, normal force (F_N) of 10N and sliding distance of 200m, 300m and 500m were done. The mass loss results are collected as seen in table 3.5. Additionally, plots of mass loss against the corresponding sliding distances are shown in figure 3.22.

Table 3.5: Mass loss (Kg) after each test at normalization temperature of 960^{O}C for the steel samples with different boron content.

Sliding Distance (m)	Mass (kg) after each test		
	31	32	33
200	0.0000144	0.0000107	0.0000105
300	0.0000259	0.0000191	0.0000209
500	0.000038	0.0000273	0.0000341

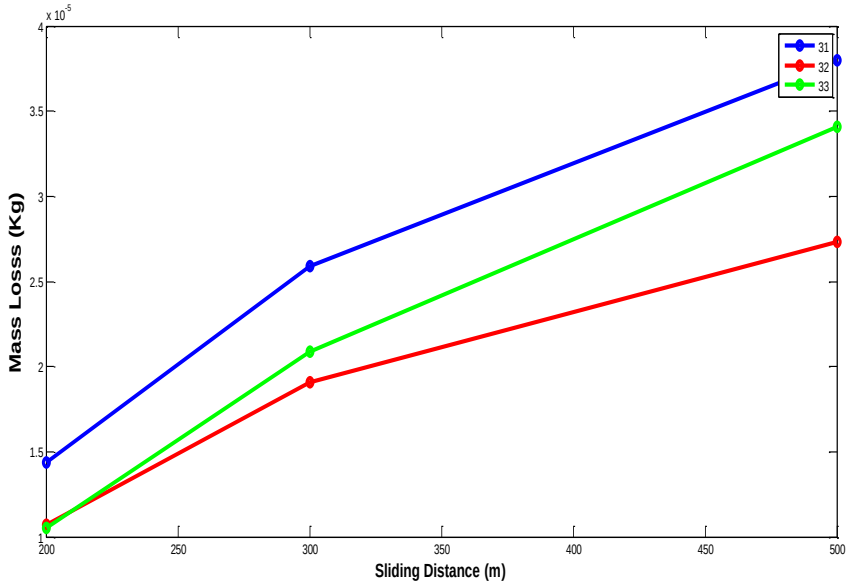

Figure 3.22: Graph of mass loss against corresponding sliding distance at normalization temperature of 960^{O}C.

Plots of the graph show uniform increase in the mass against the sliding distance. More uniformity is obtained in the mass loss with the 960^{o}C normalized steel sample, with a little variation of the mass loss at 300m sliding distance when compared to that of the as-received state.

3.3.2.2 Comparison between coefficient of friction of 31, 32 and 33 steel samples for as-received state with sliding distance of 300m and normal force (F_N) of 5N each.

Comparison between coefficient of friction against sliding distance of 31, 32 and 33 steel samples for as-received state, with sliding distance of 300m, normal force of 5N each have been investigated. For the three set of results obtained, the coefficient of friction varies because of the differences in the boron content with 31 steel sample having maximum coefficient of friction of 0.785. For steel sample with 13.5ppm of boron i.e., 32 steel sample, the maximum coefficient of friction was 0.604 and 33 steel sample with maximum coefficient of friction of 0.667. Figure 3.23 shows the graph of coefficient of friction against sliding distance of 31, 32 and 33 steel samples for as-received state, with a sliding distance of 300m and normal force (F_N) of 5N.

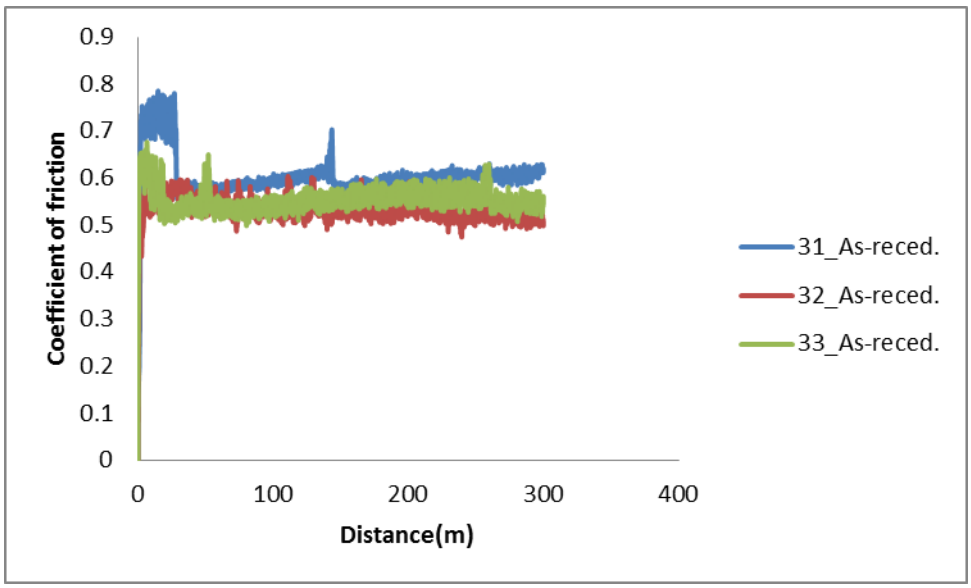

Figure 3.23: The graph of coefficient of friction against sliding distance of 31, 32 and 33 steel samples for as-received state, with a sliding distance of 300m and normal force (F_N) of 5N.

3.3.2.3 Comparison between coefficient of friction of 31, 32 and 33 steel samples with normalization temperature of 960°C, sliding distance of 300m and normal force (F_N) of 10N each.

Comparison between coefficient of friction of 31, 32 and 33 steel samples with normalization temperature of 960°C, sliding distance of 300m and normal force (F_N) of 10N each were done. The result shows at normalization of 960°C, steel sample with 13.5ppm of boron have the best maximum coefficient of friction of 0.59 when compared to other steel samples with the same processes. Additionally, the 32 steel sample has a peak within 100m sliding distance and uniform coefficient of friction between 100m to 300m sliding distance. This happens as a result of uneven distribution of boron atom within the top layer of the steel sample when compared to the distribution deep in the sample and the rate of de-oxidation. Figure 3.24 shows the graph of coefficient of friction against sliding distance of 31, 32 and 33 steel samples which are normalized at 960°C, with a sliding distance of 300m and normal force (F_N) of 10N.

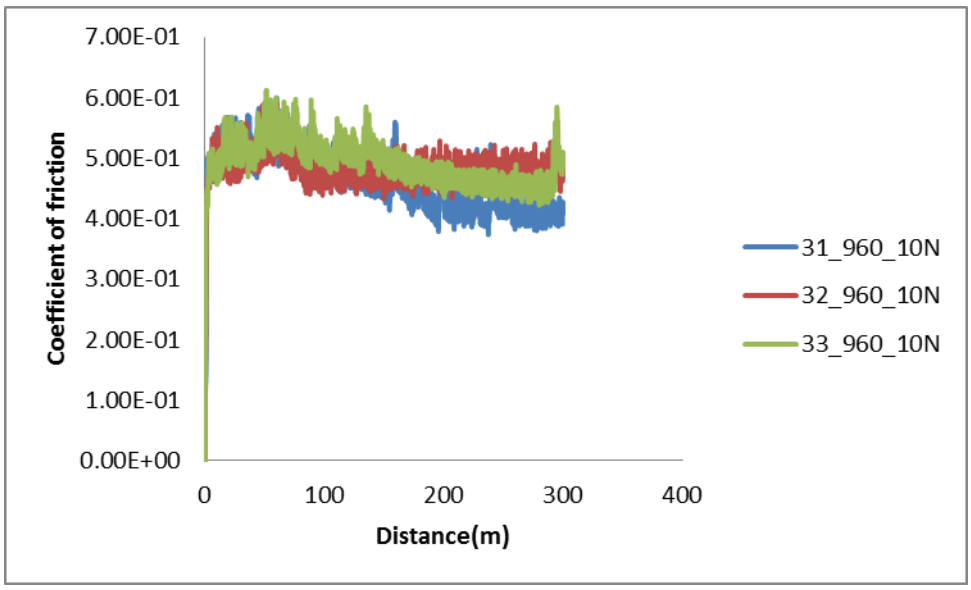

Figure 3.24: The graph of coefficient of friction against sliding distance of 31, 32 and 33 steel samples with normalization temperature of 960°C, sliding distance of 300m and normal force (F_N) of 10N.

3.3.2.4 Comparison between coefficient of friction of 31, 32 and 33 steel samples with normalization temperature of 960°C, sliding distance of 500m and normal force (F_N) of 10N each.

Comparison between coefficient of friction of 31, 32 and 33 steel samples with normalization temperature of 960°C, holding time of 45 minutes, sliding distance of 500m and normal force (F_N) of 10N each were done. With 500m sliding distance and same normalization parameters, uniform coefficient of friction is obtained with the steel samples with little peaks due to distribution of boron atoms. 31 steel sample has maximum coefficient of friction of 0.624, while 32 steel sample has maximum coefficient of friction of 0.602 and 33 steel sample it maximum coefficient of friction of 0.511 as shown in figure 3.25. It clearly indicates from the result that with 960°C normalization temperature and normal force of 10N, steel sample with 29.6 ppm of boron has more resistance to wear than the subsequent steel samples with different content of boron. Figure 3.25 shows the graph of coefficient of friction against sliding distance of 31, 32 and 33 steel samples which are normalized at 960°C, with a sliding distance of 500m and normal force (F_N) of 10N each.

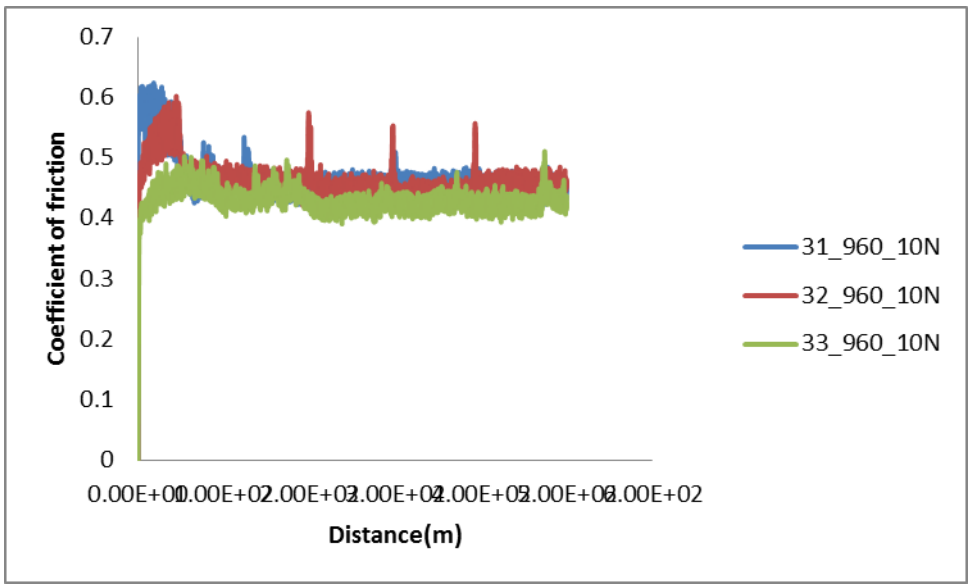

Figure 3.25: The graph of coefficient of friction against sliding distance of 31, 32 and 33 steel samples with normalization temperature of 960°C, sliding distance of 500m and normal force (F_N) of 10N.

3.3.2.5 Comparison between coefficient of friction of 31, 32 and 33 steel samples with normalization temperature of 1010°C, sliding distance of 300m and normal force (F_N) of 15N each.

Comparison between coefficient of friction of 31, 32 and 33 steel samples with normalization temperature of 1010°C, sliding distance of 300m, with an increment in the normal force (F_N) to 15N each were done. The maximum coefficient of friction of 31 steel sample is 0.545, for 32 steel sample it is 0.699 and that of 33 steel sample is 0.62. This show that 31 steel sample with 3.3ppm of boron has more wear resistance properties when normalized at 1010°C as a result of high normalization temperature which has an adverse effect on the boron. Careful usage of the normalization temperature should be made i.e. normalization temperature should not be above the A_3 temperature. Figure 3.26 shows the graph of coefficient of friction against sliding distance of 31, 32 and 33 steel samples which are normalized at 1010°C, with a sliding distance of 300m and normal force (F_N) of 15N each.

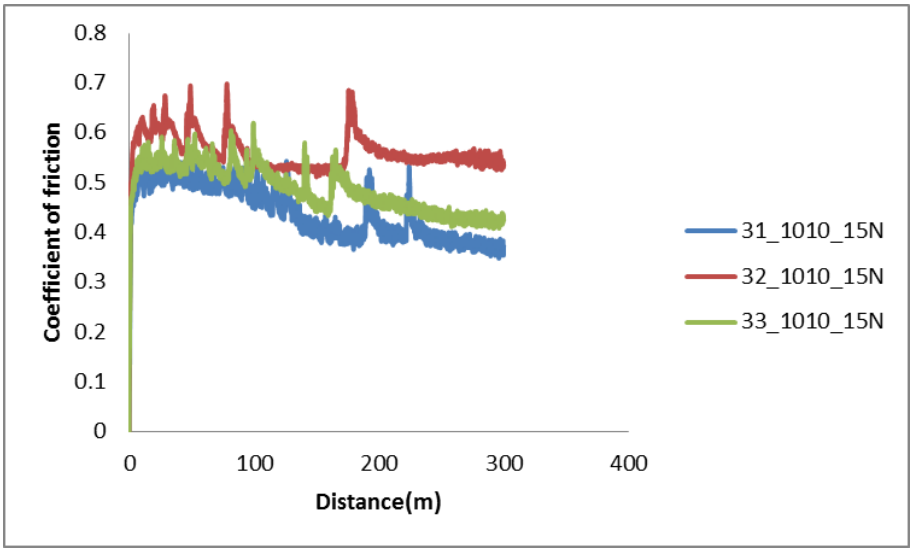

Figure 3.26: The graph of coefficient of friction against sliding distance of 31, 32 and 33 steel samples with normalization temperature of 1010°C, sliding distance of 300m and normal force (F_N) of 15N.

Table 3.7 shows the summary of the wear results obtained.

Table 3.6: Wear Test Results

Designation	Max. Frictional Force (N)	Max. Coeff. Friction	Time (Min.)	Distance (m)	Normal Force (N)
31_As-received	3.927	0.785	99.999	300	5
32_As-received	3.021	0.604	100	300	5
33_As-received	3.384	0.667	100	300	5
31_960°C	5.996	0.6	100	300	10
32_960°C	5.901	0.59	99.999	300	10
33_960°C	6.117	0.612	100	300	10
31_1010°C	8.17	0.545	99.999	300	15
32_1010°C	10.48	0.699	100	300	15
33_1010°C	9.299	0.62	99.999	300	15
31_960°C	6.242	0.624	166.667	500	10
32_960°C	6.022	0.602	166.666	500	10
33_960°C	5.11	0.511	166.667	500	10

CHAPTER 4

CONCLUSION

This chapter concludes the results obtained in the microstructural examinations of both the as-received and normalized states. Additionally, the mechanical properties of the steel sample with different content of boron. The maximum hardness of 262.4HBN for the 13.5 ppm boron steel at normalization temperature of 960^{O}C when compared to the amount of soluble boron shows that the content of the dissolved boron did not exceed that needed for the decrease of the boundaries energy in regions with ferrite formations. Normalization at higher temperatures with lower carbon content show low hardness from the measured hardness of 1010^{O}C and 1060^{O}C when compared to the as-received state. Samples heat treated at 45 minutes with 3.3 ppm, 13.5 ppm and 29.6 ppm of boron have oriented microstructures with grains and grain boundaries clearly seen. For the as-received and samples with 43.7 ppm and 58 ppm of boron have elongated and deformed grains. Considering the presence of this element boron and diminishing the energy of grain boundaries, then assumptions will be made that the largest amount of boron will be seen in areas with multiple faults, where the constitution of ferrite is the most likely. Hence, maximum hardenability in boron steel with explicitly composition in particular hardening conditions is achieved if the cognitive content of soluble boron did not surpass that needed for the decrease of the boundaries energy in areas having ferrite constitutions [6].

Boron steel samples were controlled cooled with cooling rates of 20^{O}C/min, 70^{O}C/min and 130^{O}C/min to investigate the transformation of austenite to martensite and its hardenability. For the controlled cooling process, the microstructure images of 130^{O}C/min cooling rate are predominantly of martensite structure as can be seen from the microstructure and signifies more transformation of austenite to martensite and also prove the existence of smaller grains as compared to 20^{O}C/min and 70^{O}C/min cooling rates. Additionally, other phases in the steel microstructures are observed. These phases include the lath type martensite, Widmanstätten ferrite and pearlite. Result of the variation in the supply of argon protective gas of 20^{O}C/min and 70^{O}C/min cooling rate reveal the rate of decarburization with a difference of 5.6HV.

Results of the wear properties shows steel samples normalized at 960°C with 13.5 ppm and 29.6 ppm of boron show good wear properties as compared to as-received state of the steel samples. This increase in wear properties is due to the transformation of austenite to martensite and distribution of boron atoms and also boron content in the steel sample. Coefficient of friction of 3.3 ppm, 13.5 ppm and 29.6 ppm of boron with same wear parameters and 960°C normalization temperature with a normal force of 10N shows that 13.5 ppm of steel sample has the best coefficient of friction due to its much hardenability as compared to 3.3 ppm and 29.6 ppm of boron.

REFERENCES

[1] S. Frydman, L. Konat, B. Letkowska, Pekalski., "Impact resistance and fractography of low-alloy martensitic steels", *Arch. Of Foundry Eng., spec.* Vol.8, No. 1, pp. 89-94, 2008.

[2] V.I. Arkharov, The Theory of Microalloying of Alloys, [in Russian], Mashinostroenie, Moscow, 1975.

[3] M. A. Krishtal, L. I. Ivanov and E. M. Grinberg, "Distribution of Boron in the Microstructure of a Metal", *Metalloved. Term. Obrab.* Met., No. 8, pp. 74-76, 1970.

[4] I. I. Frantov, N. I. Karchevskaya, S. A. Golovatenko, and A. V. Rudchenko," Structure and Properties of 16G2 and 16GFR Steels after Hardening and short-term Tempering",*Metalloved Term. Obrab*. Met., No. 1, pp. 50-51, 1979.

[5] A. Moria, "Properties of Boron Steels", *Neru Ser,* Vol. 18(1), pp. 42-48, 1979.

[6] I. I. Frantov, Influence of Carbon and Boron on Phase transitions in low-alloy Steels, High-Grade Steels and Alloys [in Russian], Metallurgiya, Moscow, 1978.

[7] M. P. Seah, *Acta Metall*. Vol. 28, pp. 955, 1980.

[8] T. Takamitsu, S. Hideo, T. Hiroshi, S. Yasuhiro and H.Yasushi, "TLP Diffusion Bonding of Structural Steel", *Front of Research on Behavior of Boron in Steels*: pp. 189–191, 2003.

[9] R. A. Grange and J. B. Mitchell, Trans. ASM 53 (196) 157.

[10] E. Boyle, D. O. Northwood, R. Bowers, X. Sun and P. Bauerle, "The Effect of Initial Microstructure and Heat Treatment on the Core Mechanical Properties of Carburized Automotive Steels", *Materials Forum* Vol. 32, 2008.

[11] K. Seto, D. J. Larson, P. J. Warren and G. D. W. Smit, *Scr. Mater*. Vol. 40, pp. 1029, 1999.

[12] G. E. Totten, L. Xie and K. Funtani, Handbook of Mechanical Alloy Design, CRC Press, p. 236, 2004.

[13] Classification of carbon and Low-Alloy Steels retrieved 2008-10-06.

[14] High Strength Low-Alloy Steel, 2002-11-15, archived from the original on 2010-01-03, retrieved 2008-10-11.

[15] P. Degarmo, E. Paul, J. T. Blacka and A. Ronald. *Materials and Processes in Manufacturing (9th ed. Wiley)*, ISBN 0-471-65653-4. p. 116. 2003.

[16] E. Oberg, et al. *Machinery's Handbook* (25th ed.), Industrial Press Inc. 1996.

[17] "Stainless Steel Properties for Structural Automotive Applications" Euro Inox. June 2000. Retrieved 2007-08-14.

[18] R. F. Barron, "Conference on Manufacturing Strategies", *Materials Improvement, Inc.*, Nashville, 1996, Vol. 6, pp. 535.

[19] R. F. Barron, *Preliminary Report on Effect of Cryogenic Treatment on the Wear Resistance of Tool Steels*, Materials Improvement, Inc., Hazel Park, Michigan 1974.

[20] R. F. Barron, *Dry Cryogenic Treatment Increase Machine Tool Life*, Box-board containers, 1980.

[21] N. Sasinowski, "Dimensional Tolerances and Gauging for Tooling in the Can-Making Industry", *SME Technical Paper*, MR74-945.

[22] R. Frey, *Industrial Heating*, pp. 21, September 1983.

[23] M. Kosmowski, "The Carbide and Tool Journal", Nov/Dec. 1981.

[24] *Cowles Superior Metal Cutting Tools Brochure*, Company Literature.

[25] T. P. Sweenley, *Heat Treating*, pp. 28. Febuary, 1986.

[26] P. Paulin, *Gear Technology*, pp. 23, March/April 1993.

[27] P. C. Miller, *Tooling and Production*, pp. 82, February 1980.

[28] ASM, Metals Handbook, Vol. 4, Tenth Edition, Quenching of Steel. Pp. 67, 1991.

[29] D. A. Porter and K. E. Easterling, Phase Transformations in Metals and Alloys, Second Edition, Chapman & Hall London, 1992.

[30] G. Dieter, Mechanical Metallurgy, Third Edition, McGraw-Hill, University of Maryland, 1986.

[31] ASM, Metals Handbook, Vol. 1, Tenth Edition, Medium Carbon and Low Alloy Steels. pp.432, 1990.

[32] k. Thelning, Steel and its Heat Treatment, Second Edition, pp. 240-252, 1984.

[33] R. W. Cahn and P. Haasen, Physical Metallurgy, Vol. II, Fourth Edition, Elsevier Science B. V., Amsterdam, 1996.

[34] A. K. Sinha, Ferrous Physical Metallurgy, Butterworth Publishers, Stoneham, M. A. 1989.

[35] R. W. K. Honeycombe Steels: Microstructure and properties, Edward Arnold, London, 1990.

[36] ASM, Metals Handbook, Vol. 4, Tenth Edition, Heat Treating of Steels, pp. 83-84, 1991.

[37] W. D. Callister, Jr, Materials Science and Engineering, Sixth Edition, John Wiley & Sons, Inc. 2003.

[38] ASM, Metals Handbook, Vol.4, Tenth Edition, Tempering of Steel, pp. 121-124, 1991.

[39] R. E. Reed Hill, Physical Metallurgy Principles, Princeton, New Jersey, USA, 1973.

[40] Private correspondence, Technical Forum 00-1 Retained Austenite: it's impact on Bearing Performance, BRENCO inc. (www.brencoqbs.com). A Discussion of Retained Austenite. Daniel H. Herring |630.834.3017| dherring@heat-treat-doctor.com

[41] W. Steven and A. G. Haynes, "The Temperature of Formation of Martensite and Bainite in Low-Alloy Steel", J.I.S.I., 203, 1965.

[42] D. P. Koistinen and R. E. Marburger, "A general Equation for Austenite – Martensite Transformation in Pure Carbon Steels", *Acta Metallurgia*, pp. 59-60, 7, 1959.

[43] D. Das, A. K. Dutta, K. K. Ray. "Sub-zero Treatments of AISI D2 Steel: Part 1. Microstructure and Hardness", *Journal of materials science and enginerring*, A 527 pp. 2182-2193, 2010.

[44] Y. Yalçın, "Ostemperlenmiş Küresel Grafitli Dökme demirde Kalıntı Östenit Miktra rının X-ışını Difraksiyonu İle Belirlenmesi" *Metal Dünyası*, sayi 68, 31-34, 1999.

[45] A.K.Ü. *An Investigation of Retained Austenite Contents in Carburized SAE 8620 Steel*, M.S. Thesis, Böl., 64300, Uşak, Müh. Fak. Makine Müh: TÜRKIYE: pp. 103-113 2004.

[46] G. Krauss, "Microstructure and Performance of Carburized Steel: Part 3", *adv. Matl. And Proc.* (HTP), 148, 1995.

[47] Heat Treater's Guide, *Practices and Procedures for Iron and Steels*, ASM International, pp.12, 1995.

[48] R. E. Smallman, *Modern Physical Metallurgy*, London, Butterworth, pp. 329, 1962.

[49] C. Moore, *Development of the BOC Ellenite Process (Cold Treatment of Metals with Liquid Nitrogen).* Heat Treatment 73, The Metals Society, Book No. 163, pp.157-161, 1975.

[50] F. B. Abudiana, "On the Stabilization of Retained Austenite", *Journal of Engineering Research*, Issue 5,6, March 2006.

[51] C. H. Surberg, P. Stratton and K. Lingenhöle, "The Effect of Deep Cold Treatment on two Case Hardening Steels", *Acta Metallurgia sinica*, Vol. 21(1), pp. 1-7, 2008.

[52] P. Lynwander, *Gear Drive Systems: Design and Application*, CRC Press, pp. 255, 1983.

[53] Z. L. Xie, Y. Liu and H. Haeninen, "Stabilization of Retained Austenite due to Partial Martensitic Transformation", *Acta Metallurgica et Materialia*, Vol. 42(12), pp. 4117-4133, 1994.

[54] S. J. Kim, C. J. Lee and T. H. Lee, "Effect of Cu, Cr and Ni on Mechanical Properties of 0.15 wt % C TRIP-aided Cold Rolled Steels, *Scripta Materialia*, Vol. 48(5), pp. 539-544, 2003.

[55] H and M Analytical Services, Inc. 2003. *Retained Austenite Analysis*, Hutchinson Road Allentown, NJ 08501-1415, www.h-and-m-analytical.com .

[56] ASM, Metal Handbook, Heat Treating, Vol. 4, Metals Handbook 8th Ed., ASM International.

[57] Heat Treater's Guide: Practices and procedures for Irons and Steels, ASM International, 1995, PP 12.

[58] ASM, Metal Handbook, Heat Treating, Vol. 4, Metals Handbook 8th Ed., ASM International.

[59] Handbook of Chemistry and Physics, 62nd edition, CRC Press, 1981-1982, PP. D161-D162.

[60] T. Holm, *Cryotreatment-state of the art*, AGA Internal Report, 1997-an update.

[61] D. N. Collins and J. Dormer, *Heat Treatment of Metals*, No.3, 1997.

[62] J. S. Kirkaldy and S. E. Feldman, *Journal of Heat Treating*, Vol. 7(1), pp. 57-64. 1989.

[63] V. Rudnev, D. Loveless, R. Cook and M. Black: *Handbook of Induction Heating*, Marcel Dekker, Inc., New York, 2003, pp. 39-43.

[64] A. Deva, V. Kumar, K. De Saikat, B. K. Jha and S. K. Chaudhuni, "Materal and Manufacturing Process", Vol.25, pp. 99, 2010.

[65] S. K. De, A. Deva, S. Mukhoadhyay, B. K. Jha and S. K. Chaudhuni, Steel India, No. 29, pp. 62, 2007.

[66] J. M. Challen, P. L. B. Oxley, and B.S. Hockenhull, "Prediction of Archard's Wear Coefficient for Metallic Sliding Friction assuming a Low Cycle Fatigue Wear Mechanism", *Wear*, Vol. 111, pp. 275-288, 1986.

[67] P. Maitrepierre, D. Thivellier and R. Tricot, "Influence of Boron on the Decomposition of Austenite in Low Carbon Alloyed Steels", *Metallurgical Transactions A*. 1975; 6:287-301.http://dx.doi.org/10.1007/BF02667283

[68] S. J. Cararin. *Caracterização da temperabilidade de um aço C-Mn microligado ao boro, através de dilatometria e curvas de transformações de fases por resfriamento continuo*, M.S. Thesis, São Carlos: Universidade de São Paulo, 1996.

[69] C. A. Suski, C. A. S de Oliveira "Effect of Austenitization Temperature on the Microstructure of 15BCr30 and PL22 Boron Steels", *Mat. Res.* Vol. 16, No. 4, 2003.

[70] C. Çarboğa, B. İnem and S. İmer, "The Effect of Hardening Heat Treatment on AISI 1022 Steel containing 15 and 26 ppm Boron, Technology", Vol. 13(3), pp. 139-144, 2010.